NASA Contractor Report 3119

Design and Wind Tunnel Tests of Winglets on a DC-10 Wing

R. D. Gilkey

CONTRACT NAS1-14743
APRIL 1979

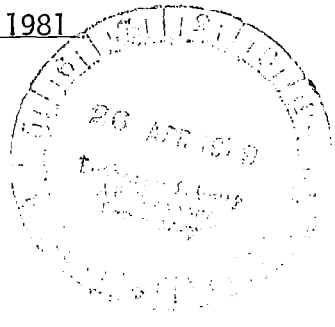

NASA

NASA Contractor Report 3119

Design and Wind Tunnel Tests of Winglets on a DC-10 Wing

R. D. Gilkey
McDonnell Douglas Corporation
Long Beach, California

Prepared for
Langley Research Center
under Contract NAS1-14743

National Aeronautics
and Space Administration

**Scientific and Technical
Information Office**

1979

FOREWORD

This document presents the results of a contract study performed for the National Aeronautics & Space Administration (NASA) by the Douglas Aircraft Company, McDonnell Douglas Corporation. This work was part of the Energy Efficient Transport (EET) project of the Aircraft Energy Efficiency (ACEE) program. The study consisted of the winglet investigations in the EET contract "Selected Winglet and Mixed Flow Long Duct Nacelle Development for DC-10 Derivative Aircraft." The activity included winglet wind tunnel development work as applied to the DC-10, oriented towards achieving the cruise drag reduction potential indicated by analytical estimates and the test experience of the NASA.

TABLE OF CONTENTS

LIST OF FIGURES

LIST OF FIGURES (Cont'd)

SYMBOLS

The longitudinal aerodynamic characteristics presented in this report are referred to the stability-axis system. Force and moment data have been reduced to coefficient form based on trapezoidal wing area. All dimensional values are given in both International System of Units (SI) and U.S. Customary Units, the principal measurements and calculations using the latter (see reference 1).

Coefficients and symbols used herein are defined as follows:

b_A wing semispan of the DC-10 Series 10, 111.29 cm (43.81 in.)

b_B wing semispan of the DC-10 Series 30/40, 118.45 cm (46.63 in.)

C_D drag coefficient, $\frac{Drag}{q_\infty S}$

ΔC_D incremental drag coefficient

C_L lift coefficient, $\frac{Lift}{q_\infty S}$

C_P pressure coefficient, $\frac{P_l - P_\infty}{q_\infty}$

c local chord, cm (in.)

$\bar{c}_A$ mean aerodynamic chord of the DC-10 Series 10 wing, 35.90 cm (14.13 in.)

$\bar{c}_B$ mean aerodynamic chord of the DC-10 Series 30/40 wing, 35.31 cm (13.90 in.)

c_l section lift-force coefficient, obtained from c_n

c_n section normal-force coefficient, obtained from integrating measured pressures

c_y section side-force coefficient, obtained from c_n

h winglet vertical height above wing-tip (see figures 8 through 11), cm (in.)

M_∞ free-stream Mach number

P_l local static pressure, Pa (lb/ft^2)

P_∞ free-stream static pressure, Pa (lb/ft^2)

q_∞ free-stream dynamic pressure, Pa (lb/ft^2)

S	DC-10 Series 10 Wing - Trapezoidal wing area - 0.7285 m^2 (7.8420 ft^2)
	DC-10 Series 30/40 Wing - Trapezoidal wing area - 0.7485 m^2 (8.0574 ft^2)
x	chordwise distance aft of leading edge, cm (in.)
y	spanwise distance from fuselage centerline, positive outboard, cm (in.)
z	vertical coordinate of airfoil, positive upward, cm (in.)
$\eta_{winglet}$	percent of winglet semispan measured from h=0 reference in figures 8 through 11.

SUMMARY

This report presents the results of a wind tunnel test, the objective of which was to establish the cruise drag improvement potential of winglets as applied to the DC-10 wide body transport aircraft. This study was conducted as part of the NASA Energy Efficient Transport (EET) program. Winglets were investigated on both the DC-10 Series 10 (domestic) and Series 30/40 (intercontinental) configurations and compared with the Series 30/40 configuration which is the wing-tip extension for the Series 10 configuration. The investigation was conducted in the Langley Research Center 8-foot transonic pressure wind tunnel using a 4.7 percent scale semi-span model of the DC-10 transport. The major portion of the test was carried out over a Mach number range of 0.6 to 0.82 and over a lift coefficient range up to 0.60 at a constant Reynolds number of 14.8×10^6 per meter (4.5×10^6 per foot).

The results of the investigation confirm that for the DC-10, winglets provide approximately twice the cruise drag reduction of wing-tip extensions for about the same increase in bending moment at the wing-fuselage juncture. Furthermore, the winglet configurations achieved drag improvements which were in close agreement with analytical estimates. It was observed that relatively small changes in wing-winglet tailoring effected large improvements in drag and visually observed flow characteristics. Careful longitudinal spacing of the upper and lower surface winglets was shown to be important in order to prevent adverse compressibility effects. All final winglet configurations exhibited good visual flow characteristics on the wing and winglets.

INTRODUCTION

The NASA Aircraft Energy Efficiency (ACEE) Program has provided a stimulus to industry to accelerate development of technology directed toward energy savings and economic benefit. Under the ACEE Energy Efficient Transport (EET) Program the winglet concept has been selected for technology development for potential application to derivatives of the DC-10 transport.

Winglets, described in reference 2, are designed to reduce induced drag at cruise conditions. The advantage of winglets is that this drag reduction can be achieved with reduced wing-root bending moments as compared to a wing-tip extension having equivalent drag reduction. Winglets also have application to configurations where considerations of airport compatibility may limit wing span. The NASA has been conducting and sponsoring several experimental investigations of the effects of winglets on jet transport wings at high subsonic Mach numbers (references 2 through 5).

The purpose of the current investigation was to develop the full cruise drag reduction potential of winglets as applied to the DC-10 transport and to evaluate these winglets relative to a wing-tip extension. The investigation was conducted in the Langley Research Center 8-foot transonic pressure wind tunnel (hereafter referred to as LRC 8-foot wind tunnel) in October-November 1977. The major portion of the test was carried out over a Mach number range of 0.60 to 0.82 and over a lift coefficient range up to 0.60 at a constant Reynolds number of 14.8×10^6 per meter (4.5×10^6 per foot).

The investigation was conducted using a 4.7 percent scale semi-span model of a DC-10 Series 10 (domestic version) and Series 30/40 (intercontinental version) wide body transport. Winglets were evaluated on both the Series 10 and on the Series 30/40 versions of the airplane. A wing-tip extension, representing the change from the Series 10 to Series 30/40 configuration, was tested for comparison. Multiple winglet incidence angles were provided on each winglet. Configuration development changes in wing-winglet tailoring were made to effect improvements in drag and observed visual flow characteristics. The effect of the addition of the lower winglet on winglet system effectiveness was also assessed.

Aerodynamic forces, and moments, as well as wing and winglet pressure data were measured. Winglet and wing-tip extension effects on wing root bending moment were evaluated utilizing the rolling moments measured by the balance.

Appreciation is to be expressed for the contribution of NASA to the study. Particular mention should be made of Dr. Richard T. Whitcomb for his continuing technical advice and his efforts during the test; also for the effective participation of Stuart G. Flechner in conducting the test, and Sue R. Orr in writing the data reduction program and maintaining the data reduction system.

EXPERIMENTAL APPARATUS AND PROCEDURES

Test Facility

This investigation was conducted in the LRC 8-foot wind tunnel. The tunnel is a single return closed circuit, variable density, continuous flow type. The test section is 2.16m (7.1 ft) square and 5.49m (18 ft) long and is slotted in the upper and lower walls for approximately five percent porosity. The Mach number can be continuously varied from .2 to 1.2. A more detailed description of the tunnel is found in reference 6.

Model Installation

The DC-10 semi-span model was mounted inverted on the Langley 804-S balance on the righthand tunnel wall. The model was positioned with a 0.51 cm (0.20 in) gap between the model plane of symmetry and the tunnel wall.

Model alignment in pitch and roll was checked using an inclinometer on the model leveling fixture surface which was referenced to the fuselage reference plane. A drawing of the model installation is presented in figure 1.

Model Description

The basic model is a 4.7 percent scale semi-span configuration of the wide-body DC-10 jet transport. The model was tested with tail surfaces removed and a flow-through nacelle and pylon mounted on the wing. Photographs of winglets on the DC-10 model installed in the LRC 8-foot wind tunnel are presented in figures 2 through 5.

Fuselage - The fuselage of this semi-span configuration represents the true fuselage split at the centerline. This fuselage has a canopy in the nose, a cylindrical midsection, and a boattail afterbody.

Wing - The wing planform geometry is described in figure 6. This wing has 35 degrees of quarter chord sweep and six degrees of dihedral. The total trapezoidal wing aspect ratio is 6.8 for the Series 10 and 7.5 for the Series 30/40.

Wing-tip Extension - The wing-tip extension is defined as the added wing planform which converts the Series 10 to the Series 30/40 configuration. The semi-span extension is 7.16 cm (2.82 in) and is 6.4 percent of the Series 10 semi-span, or 5 feet full scale.

Winglets - The winglet is based on the design by Dr. R. T. Whitcomb of NASA Langley with general design guidelines published in reference 2. Prior to selection of test configurations, analytical studies were made using the Douglas Nonplanar Lifting Surface program (reference 7). Perturbations were made in winglet height, taper ratio, location, upper surface/lower surface combinations, and size. These analyses indicated that no significant improvements could be realized by changes to the Whitcomb design within the design guidelines utilized. All winglets utilized a NASA Langley modified GAW eight-percent thick airfoil section defined in figure 7. The upper surface of the airfoil faces inboard (toward the fuselage) on the upper winglets and away from the fuselage on the lower winglets. All upper surface winglets were mounted at a dihedral of 75 degrees (15 degrees from the vertical) and were untwisted. All lower surface winglets were mounted at an anhedral of 54 degrees (-36 degrees from the vertical) and were untwisted. Two upper- and lower-winglet system geometries were provided. One of these winglet systems was utilized on the Series 10 wing-tip while the other was utilized on the Series 30/40 wing-tip. In addition, the upper surface winglet utilized on the Series 10 configuration had the capability of being tested on the Series 30/40 wing-tip. Capability was provided to test upper and lower winglets together and with the lower surface winglet removed. The upper surface winglets could be set to winglet root airfoil incidence angles

relative to the fuselage centerline of 0, -2, or -4 degrees, where negative incidence angle is trailing edge inboard (i.e., in the direction to unload the upper surface winglet) as shown in figure 8. The lower surface winglets were set at zero degrees incidence angle. As winglet incidence angle is changed, removable wing-tip spacers prevent the wing-tip from extending beyond the outboard edge of the upper surface winglet. Detailed sketches of the winglet configurations are presented in figures 8 through 11.

DC-10 Series 10 Winglets - The winglet system for the Series 10 is designated winglet A and is shown in figure 8. The upper surface winglet has a span equal to the wing-tip chord (13.6-percent wing semispan), a root chord equal to 65 percent of the wing-tip chord, a taper ratio of 0.30, and a leading-edge sweep of 40 degrees. The lower surface winglet has a root chord of 40 percent of the wing-tip chord, a taper ratio of 0.42, and a leading-edge sweep of 52 degrees.

Development for maximum Series 10 winglet drag reduction resulted in significant changes to the winglet geometry, as shown in figure 9. The resulting configuration, referred to as winglet A1 consisted of winglet A with the lower winglet moved forward 0.51 cm (0.20 in). The leading edge of the re-positioned lower winglet was then cut back and recontoured into the leading edge of the wing-tip. A small fillet was added to the outboard intersection of the lower winglet and wing-tip. Configuration A2 consisted of configuration A1 with a small triangular shaped buildup added to the outboard surface of the upper surface winglet near the trailing edge intersection with the wing-tip. Configuration A3 consisted of configuration A2 with the upper winglet moved forward 1.81 cm (0.71 in) on the wing-tip.

DC-10 Series 30/40 Winglets - The winglet systems for the Series 30/40 are designated winglet B and C and shown in figures 10 and 11. Winglet B consists of an upper surface winglet with a span equal to the Series 10 winglet span, a root chord equal to 65 percent of the wing-tip chord, a taper ratio of 0.30 and a leading edge sweep of 39 degrees. The lower surface winglet has a root chord

of 40 percent of wing-tip chord, a taper ratio of 0.28, and a leading-edge sweep of 52 degrees. Like winglet A2, fill was added to the lower winglet wing-tip juncture and on the outboard surface of the upper winglet near the trailing edge intersection with the wing-tip (figure 10).

Winglet C configuration is defined as the winglet B configuration with the upper surface winglet replaced by winglet A2. That is, the Series 10 upper winglet is used on the Series 30/40 wing-tip. The Series 30/40 lower winglet B is retained. This results in an upper surface winglet equal to winglet B in span, a root chord equal to 77 percent of the wing-tip chord, a taper ratio of 0.30, and a leading edge sweep of 40 degrees.

Boundary Layer Transition Strips - Full span boundary layer transition strips were placed on the upper and lower surfaces of the wing and winglets. These strips were comprised of 0.16 cm (0.06 in) wide bands of carborundum grains set in a plastic adhesive. On the upper and lower wing surface inboard of the trailing edge break No. 150 grains were located at five percent chord. On the upper and lower surface of the wing outboard of the trailing edge break No. 180 grains were located at five percent chord. On the upper surface (inboard) of all upper winglets, No. 240 grains were applied at five percent chord. On the upper surface (outboard) of the lower winglets, No. 240 grains were also applied at five percent chord. On the lower surface (outboard) of all upper winglets, No. 180 grains were applied at thirty-five percent chord on the lower half of the winglet span. On the upper half of this winglet span No. 220 grains were applied at thirty-five percent chord. On the lower surface (inboard) of the lower winglets, No. 220 grains were applied at thirty-five percent chord. Boundary layer transition strips were also applied to the nacelle, pylon, and fuselage nose. The carborundum grains were sized according to the criteria of reference 8.

The transition strips on the lower surface of the winglets were located rearward in an attempt to simulate full-scale Reynolds number boundary-layer conditions (reference 9). The strips on the upper surface of the winglets were located forward to insure transition ahead of the shock for the various test conditions.

Test Conditions

The major portion of the measurements were taken over a Mach number range of 0.60 to 0.82 with the angle of attack of the model varied in approximately one half degree increments over a range corresponding to lift coefficient values between 0.40 and 0.60. A constant Reynolds number of 14.8×10^6 per meter (4.5×10^6 per foot) or 5.3×10^6 based on the mean aerodynamic chord of the DC-10 Series 10 was maintained for this investigation.

Measurements

The model was equipped for measuring force, moment, and pressure data. The force and moment data were obtained by using a five-component electrical strain-gage balance. Side force measurements were not taken. The angle of attack accelerometer was housed within the fuselage. The fuselage was mounted on the balance and no corrections were made for base or cavity pressures.

Chordwise static-pressure orifices were located at 15, 34, 55, 70, 85, and 96 percent semi-span stations of the Series 10 wing. An additional row of chordwise static pressure orifices located at 96 percent of the extended wing semi-span was included on the Series 30/40 wing. Chordwise static pressure orifices were located on the upper surface winglets at 12.5 and 80.0 percent of winglet span.

All forces, moments, and pressures were recorded on the LRC 8-foot wind tunnel 65 channel solid state high speed data acquisition system and reduced on and off site.

Repeatability of Data

The Reynolds number was held to within ±32,800 per meter (±10,000 per foot) and the Mach number to within ±0.002 of the intended values throughout the test. During the course of winglet development work, model deterioration due to erosion and vibration caused plaster fill deterioration. This resulted in small drag changes with time that were judged acceptable for winglet development but not for assessing final winglet performance increments. Final winglet and wing-tip increments were measured by cleaning up all surfaces,

filling and smoothing cracks, and re-testing this configuration with and without winglets to define the final increments. Repeat points were taken at each Mach number for all final winglet and wing-tip incremental drag performance runs. The drag coefficient repeatability was generally within ±0.0002, while lift coefficient repeated within ±0.002.

RESULTS AND DISCUSSION

The effects of the installation of winglets and wing-tip extension on the cruise drag are presented in the form of incremental drag coefficients. Since winglets and wing-tip extensions introduce pitching moment changes, which in turn, impact the longitudinal trim drag, all incremental drag results presented include trim effects. Pitching moment data were acquired and used for trimming purposes. No significant differences in pitching moment were noted between winglets and wing-tip extension configurations. These trim effects are typically one to one and one-half drag counts penalty at cruise lift coefficients. Lift data were acquired primarily for correlating drag at given values of lift.

Considerable development work, with the aid of fluorescent oil flow visualization, was necessary to achieve winglet configurations that did not experience boundary layer separation.

Winglet Development on DC-10 Series 10 - The upper and lower surface winglet A, was tested on the DC-10 Series 10 model. The upper surface winglet was tested at 0, -2, and -4 degree incidence angles; as shown in figure 8, negative angles are in the direction to reduce the loading on the upper surface winglet. Figure 12 shows the incremental winglet drag coefficient results for Mach numbers of 0.60, 0.74, and 0.82. A deterioration of the improvement is indicated with increasing Mach number. Fluorescent oil flow pictures, figure 13, indicates a high cross flow and a separated region on the outboard surface of the lower winglet at the upper trailing edge for 0.74 and 0.82 Mach numbers, but not at 0.60 Mach number. Also shown in figure 12 is the incremental effect of the upper surface winglet alone at -2 and -4 degree incidence angles for Mach numbers of 0.60, 0.74, and 0.82. Fluorescent oil flow, figure 13, indicates up-flow on the aft inboard surface of the winglet/wing juncture, increasing significantly with increasing Mach number. Apparently this caused the loss of winglet effectiveness with increasing Mach number for the -2 degree incidence angle configuration as indicated in figure 12.

At a Mach number of 0.60 both winglet configurations exhibited reasonably well behaved oil flow characteristics. Therefore, force data for these configurations at the 0.60 Mach number condition should represent the potential for these configurations allowing conclusions to be made. Both the upper-and-lower and upper-alone configurations indicated the best drag reduction at -2 degrees incidence angle. In addition, it is clear that the upper and lower surface winglet configuration offers considerably more drag reduction potential compared to the upper surface winglet alone configuration. On the basis of these results, the upper and lower surface winglet configuration at -2 degrees upper surface incidence angle was selected for further development work to eliminate the flow separation at the higher Mach numbers.

The original design intent was to have the upper winglet leading edge and lower surface winglet trailing edge intersect the wing-tip surface at the same percent wing-tip chord (thus no overlapping of upper and lower winglets). Manufacturing difficulties resulted in the upper surface winglet being shifted forward by 0.51 cm (0.20 in) producing an upper and lower surface winglet overlap as shown in figure 8. It was speculated that this overlapping

might be causing detrimental interference on the lower winglet, leading to the observed flow separation. It was not possible to relocate the upper winglet so the lower winglet was relocated 0.51 cm (0.20 in) forward to eliminate overlap with the upper winglet. As stated previously under Model Descriptions, the leading edge of this lower winglet was then cut back and recontoured into the wing-tip leading edge. A small juncture fillet was added to the lower winglet upper surface intersection with the wing. Figure 9 shows the revised test configuration A1. Figure 14 shows that the revised configuration A1 completely eliminated the flow separation.

An additional modification, A2, was made based on a type of modification developed by Dr. Whitcomb, which has been successful in obtaining further improvements on other winglet configurations. This consisted of a small triangular-shaped buildup of the outboard surface of the upper winglet near the trailing edge intersection with the wing-tip as shown in figure 9. The purpose of this modification was to produce a blunt trailing edge causing a trailing edge suction that might improve the boundary layer in the wing-winglet intersection. Configuration A2 produced approximately the same level of drag improvement as A1 at the higher Mach numbers.

Initial winglet parametric studies utilizing the Douglas inviscid Nonplanar Lifting System program, reference 7, indicated that a slight improvement of induced drag could be achieved by moving the upper winglet forward. However, reasonable care must be taken not to position the winglet too far forward in order to prevent wing and winglet peak velocity interference. Configuration A3 represents configuration A2 with the upper winglet moved forward twelve percent of wing-tip chord as shown in figure 9. Figure 15 shows that the impact of the forward movement is to cause a significant performance loss for 0.74 and 0.82 Mach numbers, indicating that the aft position was best. Oil flow visualization did not indicate any separation problems on this configuration so no further development was conducted. It was therefore concluded that the aft position was superior. For final winglet A2 increments a new baseline was run and the results are also shown in figure 15.

Chordwise pressure distributions on the best DC-10 Series 10 configuration upper surface winglet A2 are presented in figure 16. There are no indications of any flow problems on the winglet for both chordwise pressure rows. However, high leading edge upper surface peak pressures are shown for the outboard winglet chordwise pressure row ($\eta_{winglet} = 0.80$).

Spanload distributions at 0.82 Mach number and 0.5 lift coefficient are presented in figure 17 for the wing alone and for the wing with upper and lower surface winglet A2 installed. As seen in previous investigations, and predicted by methods of reference 7, the increased loading effect due to the addition of winglets is quite locally concentrated in the region of the wing-tip.

Winglet Development on DC-10 Series 30/40 - Configuration modifications for minimum upper and lower winglet overlap and additions of filleting resulting from the development work on the Series 10 winglet were incorporated into winglet B for testing on the Series 30/40. Configuration B is defined in figure 10. The upper surface winglet was tested at 0, and -2 degree incidence angles. At the cruise Mach number of 0.82, the -2 degree incidence position was slightly better. Oil flow pictures at -2 degrees incidence angle did not indicate any flow separation problems.

To increase winglet effectivness on the rather small chord wing-tip of the Series 30/40 configuration a larger chord upper surface winglet was tried. The Series 10 upper surface winglet A2 was attached to the Series 30/40 wing-tip while the lower winglet for the Series 30/40 was retained. This configuration, designated winglet C, is defined in figure 11. This results in an upper winglet root chord that is 77 percent of wing-tip chord. A comparison of incremental drag results of winglet C relative to winglet B is shown in figure 18. As shown, the large-chord winglet C demonstrated significant improvement at all three Mach numbers. Oil flow pictures indicated no flow separation on winglet C.

Apparently, upper and lower surface interference is not significant for this case with a relatively large upper and lower surface winglet overlap. For final winglet C increments the winglet configuration was run back to back with a new baseline and the results are shown in figure 18.

Chordwise pressure distributions on the best Series 30/40 configuration upper surface winglet C are presented in figure 19. There are no indications of any flow problems at either the root or tip area of the winglet. As was the case for the best Series 10 configuration the upper surface leading edge peak pressure was highest toward the tip of the winglet.

Span load distributions at 0.82 Mach number and 0.5 lift coefficient are presented in figure 20 for the wing alone and for the wing with upper and lower surface winglet C installed. As was the case for winglets on the Series 10 and seen in previous investigations, the increased loading effect due to the addition of winglets is quite locally concentrated in the region of the wing-tip.

Comparison of Estimated and Experimental Incremental Drag for Winglets and Wing-Tip Extensions - Figure 21 presents an incremental drag summary of the best Series 10 and Series 30/40 winglet and wing-tip extension wind tunnel results. In addition, comparison is made to analytical estimates. The Douglas Nonplanar Lifting Systems Method (NPLS), reference 7, was used to estimate the theoretical induced drag improvements for winglets and the wing-tip extension for a wing span loading corresponding to a 0.82 cruise Mach number condition. The parasite drag of the winglets and wing-tip extensions was estimated by standard methods utilizing appropriate form factors and with skin friction coefficients corresponding to the test conditions.

It has been found, reference 2, that the largest measured reductions of drag due to adding the winglet are obtained with normal loads on the winglet less than suggested as optimum by the theory. As loading on the winglet increases, viscous drag effects increase and can offset improvements in wing-winglet induced drag. The wind tunnel data show that the best performance is obtained with a winglet off loaded from the theoretical optimum. This is apparent from the experimental and analytical data comparison.

Two levels of winglet performance estimates are shown. The predicted optimum level from the NPLS program occurred at 0 degree upper winglet incidence angle. However, the best test winglet incidence was off-loaded by two degrees (-2 degree incidence angle). A second estimate line for the best winglet test configuration (-2 degree incidence) is also shown. The best winglets for both the Series 10 and Series 30/40 achieved drag reductions somewhat less than the full analytical potential but agreed relatively well with the estimates at the same -2 degree incidence as for the test configuration.

Figure 22 presents a comparison of the two analytical winglet loadings and the measured loadings for the best Series 10 and Series 30/40 winglets. This confirms that the best measured winglet loadings are lower than the optimum analytical loadings. For the test configuration (-2 degree incidence angle) the measured loading matched the estimated loadings reasonably well. Thus for the test configuration the analytical estimate essentially matches the wind tunnel winglet loading, figure 22, and incremental drag performance, figure 21.

The measured performance improvement for the wing-tip extension agrees well with the analytical estimate as indicated in figure 21. The wing-tip extension performance is based on Series 10 geometry. The wing span load distributions for the Series 10 and Series 30/40 at 0.82 Mach number and 0.5 lift coefficient are presented in figure 23.

Winglets and Wing-Tip Extension Data Summary - A summary of winglets and wing-tip extension drag increments are presented in figure 24. The increments are presented for a range of Mach numbers including a typical cruise Mach number of 0.82. For comparison purposes Series 10 and Series 30/40 winglet data have previously been presented at a lift coefficient of 0.50 with some figures including data over a range of lift coefficients. This summary presents incremental data for both the Series 10 and Series 30/40 each at its most representative cruise lift coefficient. The Series 10 aircraft flies at an average cruise lift coefficient of approximately 0.45. Thus, the incremental drag improvements due to the addition of the winglet or wing-tip extension are assessed at a lift coefficient of 0.45. The heavier Series 30/40 aircraft

flies at a higher average cruise lift coefficient of about 0.50. Thus, the incremental drag improvement due to the addition of a winglet on the Series 30/40 is assessed at a lift coefficient of 0.50.

A second table in figure 24 presents winglets and wing-tip extension wind tunnel increments adjusted to flight Reynolds number. Standard methods were used to adjust parasite drag of the winglets and wing-tip extension from the wind tunnel Reynolds number of 5.3×10^6 to 5.0×10^7 (based on MAC) for flight. These increments represent the winglets and wing-tip potential in flight. For the cruise conditions the incremental drag coefficient improvements for the installation of a winglet on the Series 10 and Series 30/40 are 0.0012 and 0.0010, respectively. The cruise condition incremental drag coefficient improvement for the wing-tip extension is 0.0009.

Winglets and Wing-Tip Extension Incremental Drag and Root Bending Moment Comparison - The comparative increase in wing root bending moment for winglets compared to wing-tip extensions is presented in figure 25. Measured drag improvements and measured increases in wing-root bending moment for a fixed-lift coefficient of 0.5 are presented. Also shown are measured drag increments corrected to flight Reynolds number. Regional shading of winglet performance compared with wing-tip extension performance is also shown. The increase in wing-root bending moment due to a wing-tip device is indicative of the basic wing structural weight penalty for the inclusion of the device. As indicated, for a fixed value of drag improvement, winglets produce about one-half of the increase in wing-root bending moment as wing-tip extensions. Alternately, for the same increase in wing-root bending moment, winglets provide approximately twice the drag improvements as wing-tip extensions.

CONCLUSIONS

A development test to determine the cruise drag reduction potential of winglets relative to wing-tip extensions as applied to the DC-10 transport has been conducted in the NASA Langley Research Center 8-foot transonic pressure wind tunnel. Significant results from this test indicate the following:

1) Winglets achieved drag reduction close to optimum analytical estimates. The wing-tip extension achieved the full analytical drag reduction potential.

2) Winglets provide approximately twice the cruise drag reduction obtainable with wing-tip extensions for the same increase in bending moment at the wing/fuselage juncture.

3) Small changes in wing-winglet tailoring effected significant improvements in drag and visual flow characteristics. Careful longitudinal relative spacing of the upper and lower surface winglets are shown to be important to prevent adverse compressibility effects. All final winglet configurations exhibited good visual flow characteristics on the wing and winglets.

4) Drag improvements at cruise conditions due to winglets were fairly insensitive to winglet incidence angle over a range of angles tested. However, an off-loaded position (-2 degrees upper winglet incidence) was slightly better.

REFERENCES

1. Mechtly, E. A.: The International System of Units - Physical Constants and Conversion Factors. NASA SP-7012, 1973.

2. Whitcomb, Richard T.: A Design Approach and Selected Wind Tunnel Results at High Subsonic Speeds for Wing-Tip Mounted Winglets. NASA TN D-8260, 1976.

3. Flechner, Stuart G.; Jacobs, Peter F.; and Whitcomb, Richard T.: A High Subsonic Speed Wind-Tunnel Investigation of Winglets on a Representative Second-Generation Jet Transport Wing. NASA TND-8264, 1976.

4. Jacobs, Peter F.; and Flechner, Stuart G.: The Effect of Winglets on the Static Aerodynamic Stability Characteristics of a Representative Second Generation Jet Transport Model. NASA TND-8267, 1976.

5. Jacobs, Peter F.; Flechner, Stuart G.; and Montoya, Lawrence C.: Effect of Winglets on a First-Generation Jet Transport Wing I, II, and III. NASA TND-8473, TND 8474, and TND-8478, 1977.

6. Pirrello, C. J.; Hardin, R. D.; and Heckart, M. V.: An Inventory of Aeronautical Ground Research Facilities Volume I - Wind Tunnels. NASA CR-1874, 1971.

7. Goldhammer, M. I.: A Lifting Surface Theory for the Analysis of Nonplanar Lifting Systems. AIAA Paper No. 76-16, January 1976.

8. Braslow, Albert L.; and Knox, Eugene C.: Simplified Method for Determination of Critical Height of Distributed Roughness Particles for Boundary-Layer Transition at Mach Numbers from 0 to 5. NACA TN 4363, 1958.

9. Blackwell, James A., Jr.: Preliminary Study of Effects of Reynolds Number and Boundary-Layer Transition Location on Shock Induced Separation. NASA TND-5003, 1969.

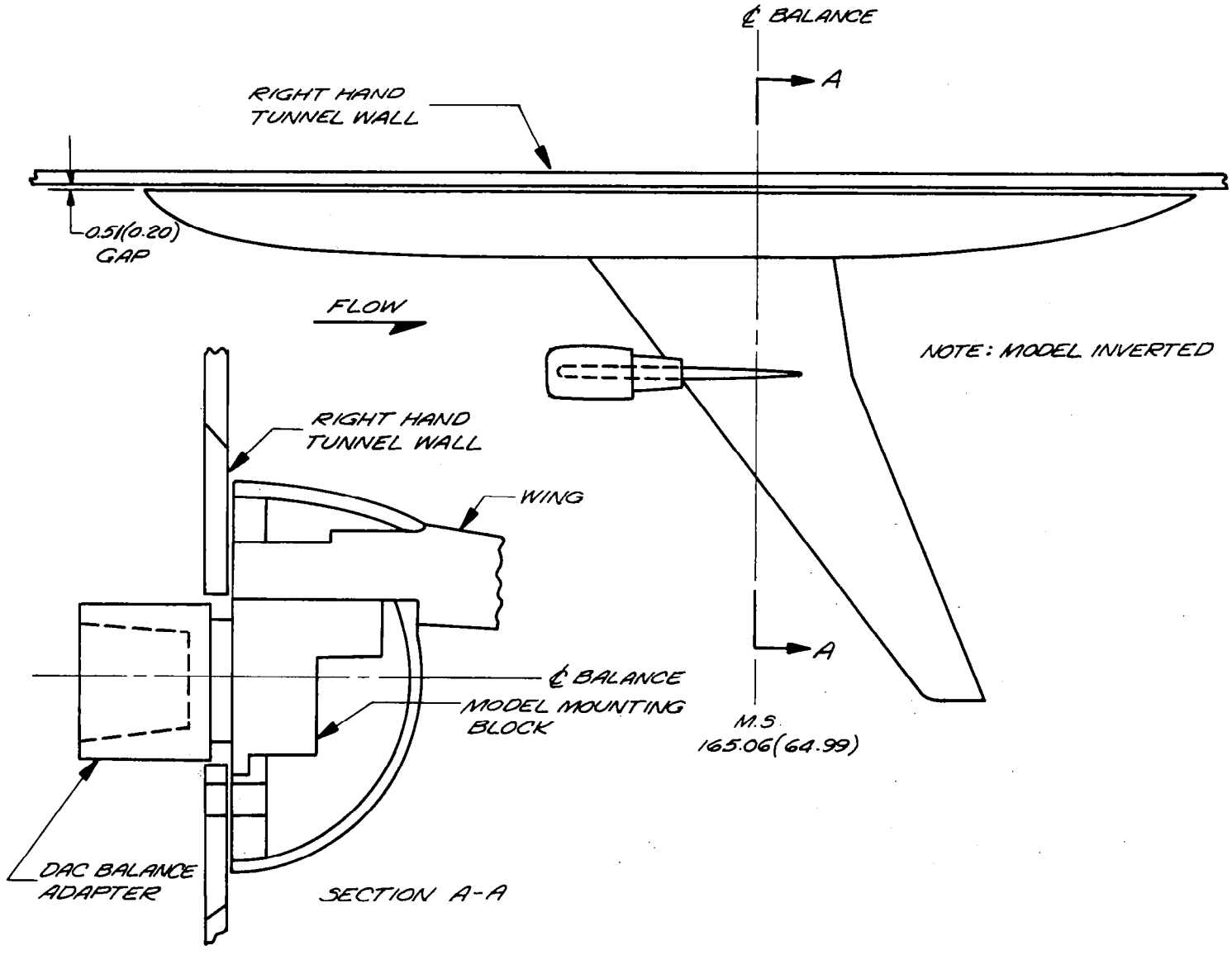

FIGURE 1. MODEL INSTALLED IN LRC 8-FT WIND TUNNEL

FIGURE 2. PHOTOGRAPH OF WINGLET A2 ON THE DC-10 SERIES 10 MODEL

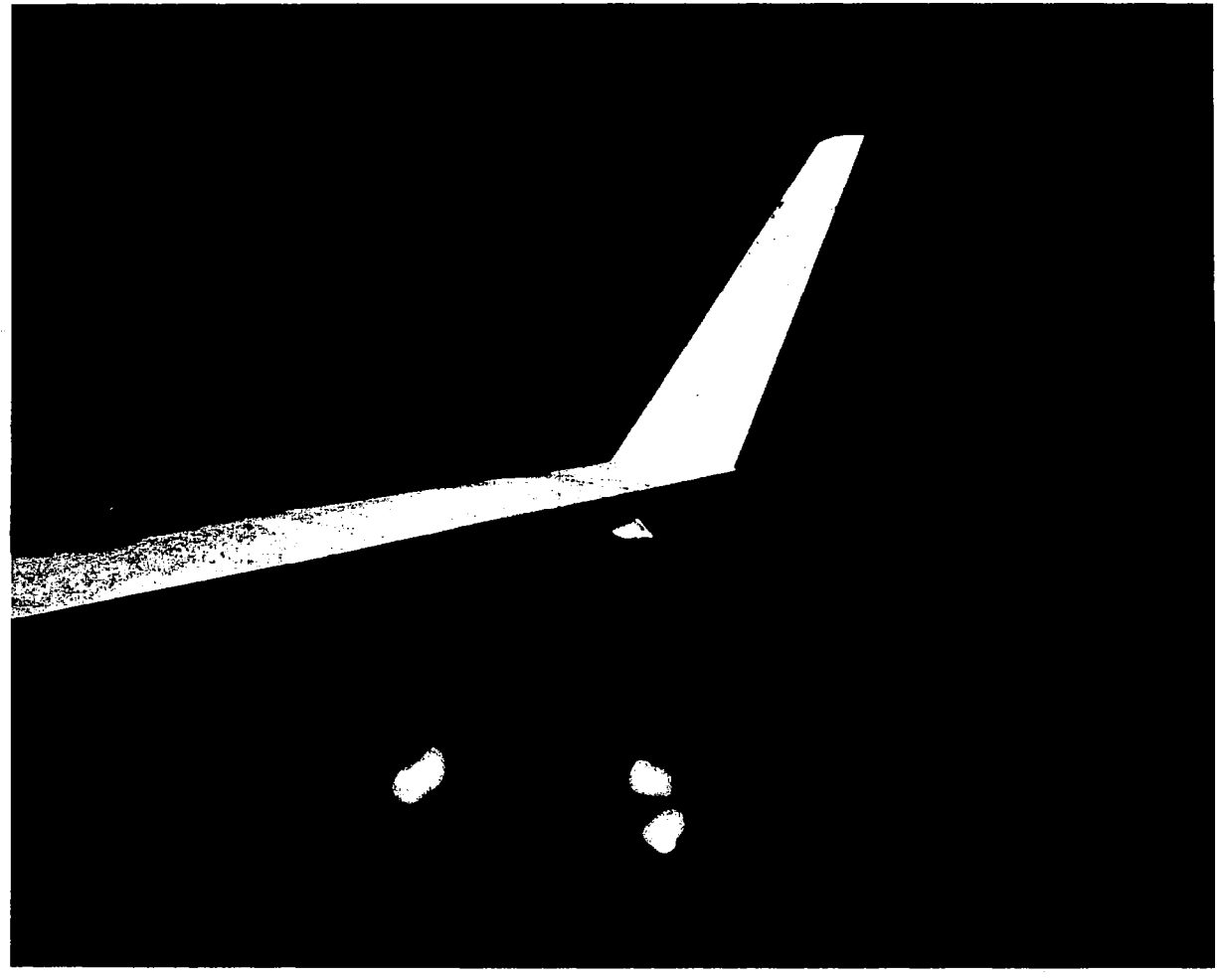

FIGURE 3. PHOTOGRAPH OF INBOARD SIDE OF WINGLET A2 ON THE DC-10 SERIES 10 MODEL

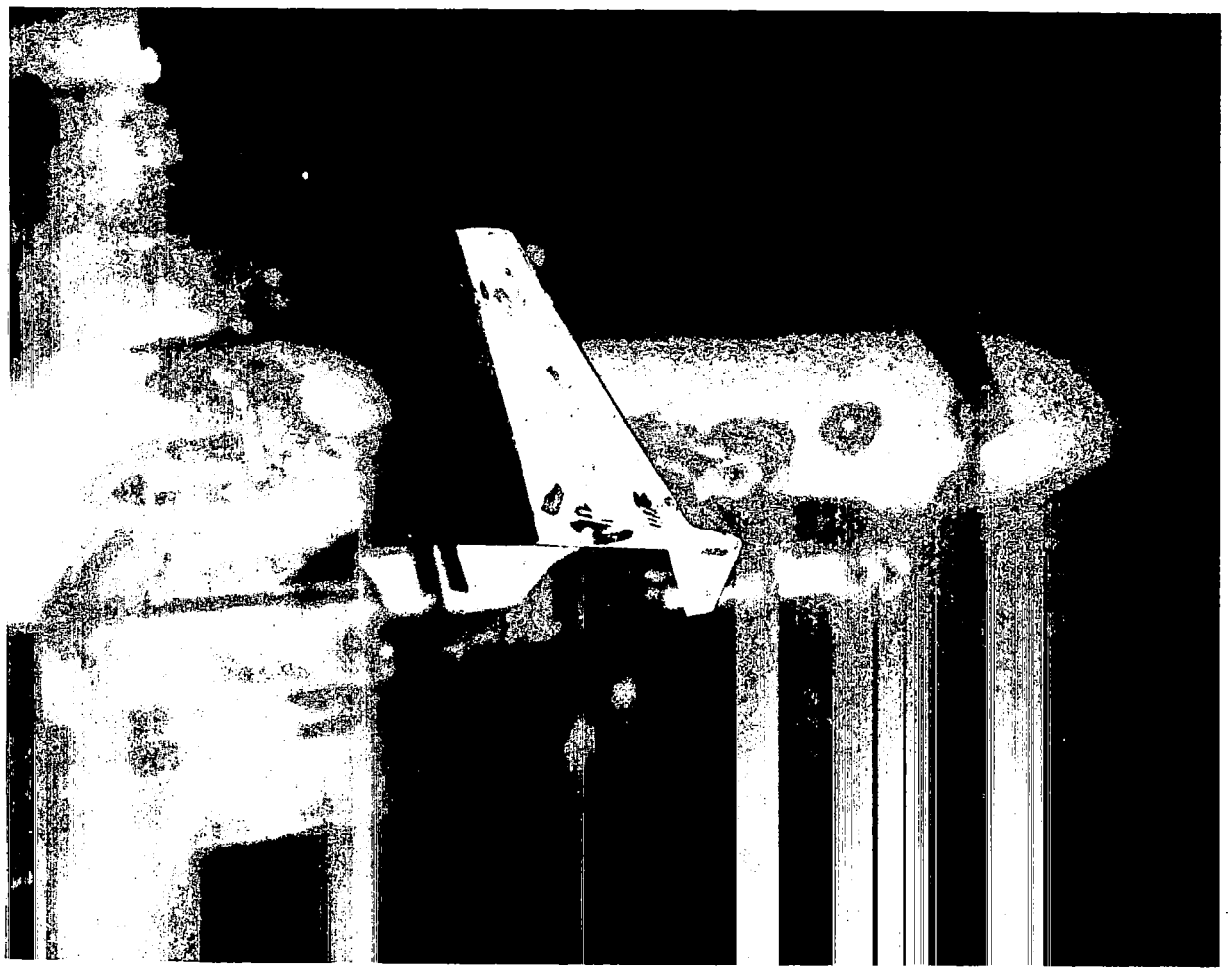

FIGURE 4. PHOTOGRAPH OF WINGLET C ON THE DC-10 SERIES 30/40 MODEL

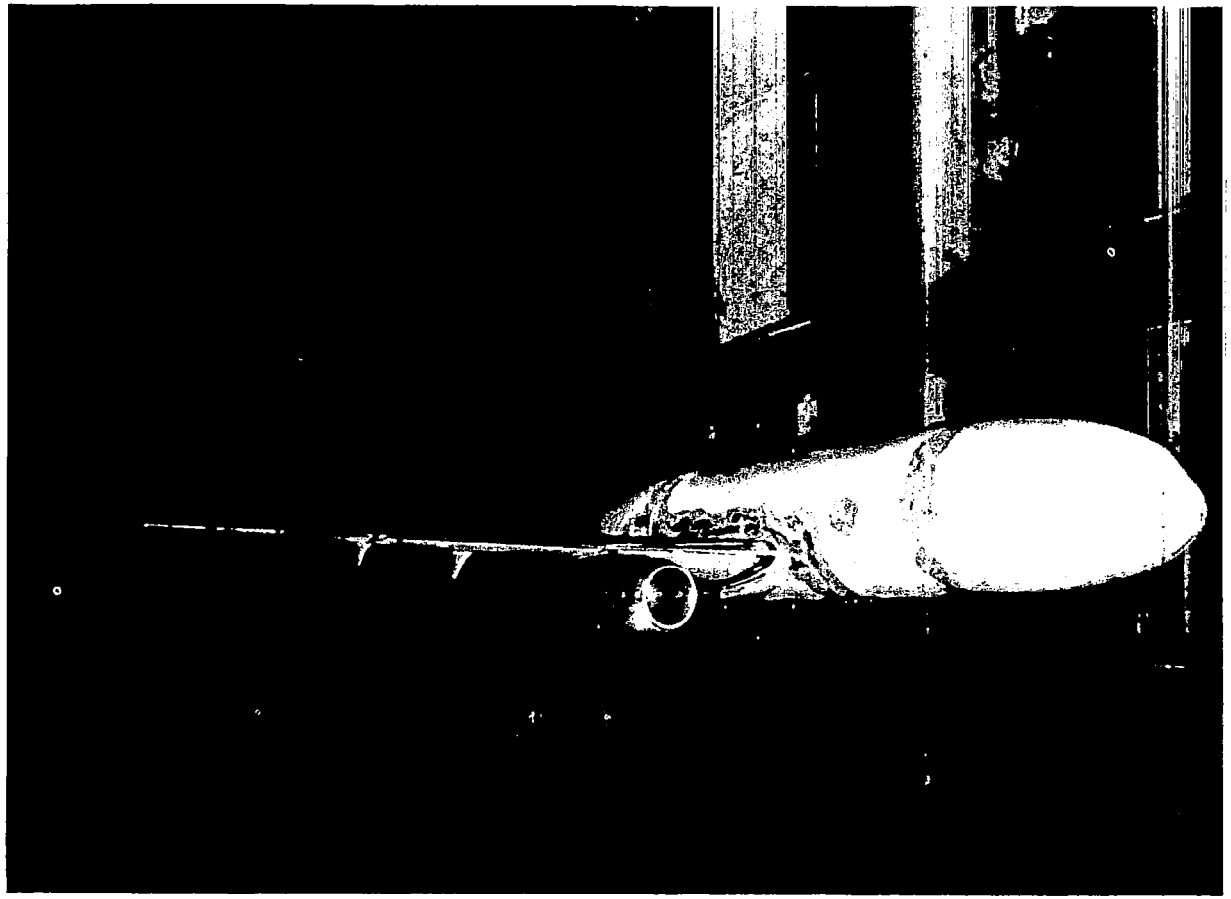

FIGURE 5. PHOTOGRAPH OF FRONT OF DC-10 SERIES 30/40 MODEL WITH WINGLET C

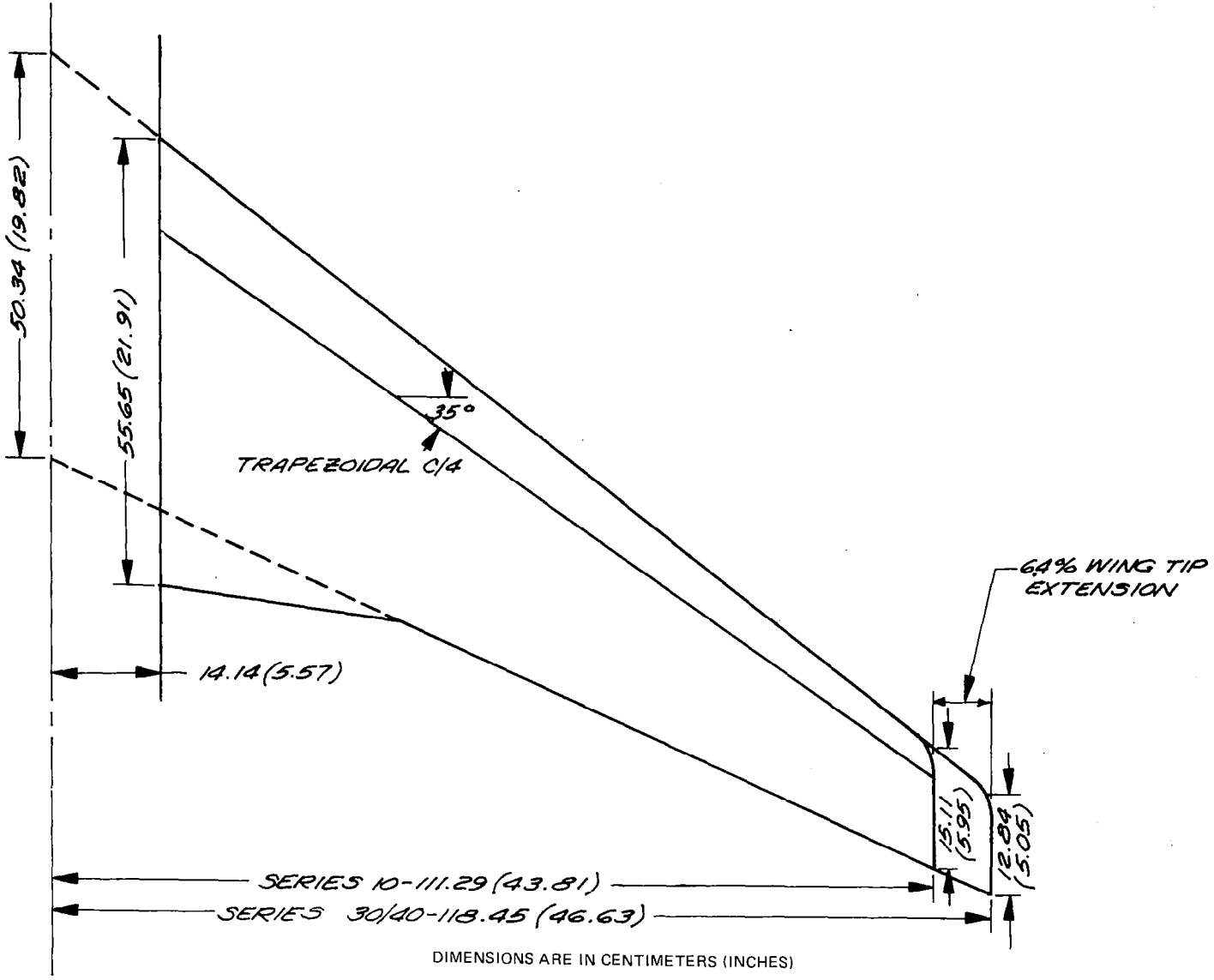

FIGURE 6. DC-10 WING GEOMETRY DEFINITIONS

NASA Langley Modified GAW Airfoil

x/c	z/c for –	
	Upper surface	Lower surface
0	0	0
.0020	.0077	-.0032
.0050	.0119	-.0041
.0125	.0179	-.0060
.0250	.0249	-.0077
.0375	.0296	-.0090
.0500	.0333	-.0100
.0750	.0389	-.0118
.1000	.0433	-.0132
.1250	.0469	-.0144
.1500	.0499	-.0154
.1750	.0525	-.0161
.2000	.0547	-.0167
.2500	.0581	-.0175
.3000	.0605	-.0176
.3500	.0621	-.0174
.4000	.0628	-.0168
.4500	.0627	-.0158
.5000	.0618	-.0144
.5500	.0599	-.0122
.5750	.0587	-.0106
.6000	.0572	-.0090
.6250	.0554	-.0071
.6500	.0533	-.0052
.6750	.0508	-.0033
.7000	.0481	-.0015
.7250	.0451	.0004
.7500	.0419	.0020
.7750	.0384	.0036
.8000	.0349	.0049
.8250	.0311	.0060
.8500	.0270	.0065
.8750	.0228	.0064
.9000	.0184	.0059
.9250	.0138	.0045
.9500	.0089	.0021
.9750	.0038	-.0013
1.0000	-.0020	-.0067

FIGURE 7. WINGLET AIRFOIL COORDINATES

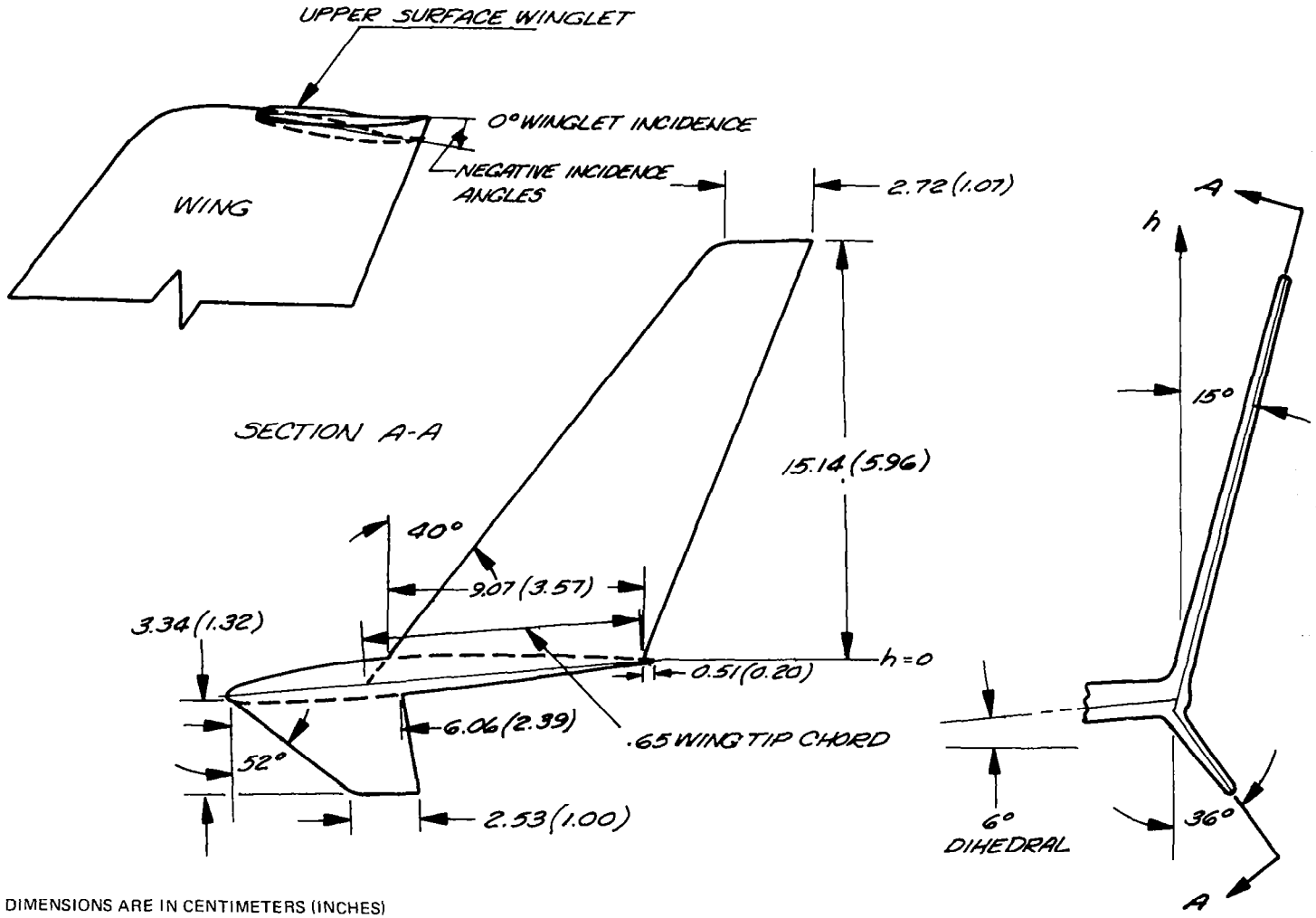

DIMENSIONS ARE IN CENTIMETERS (INCHES)

FIGURE 8. GEOMETRY DEFINITION OF WINGLET A INSTALLED ON DC-10 SERIES 10

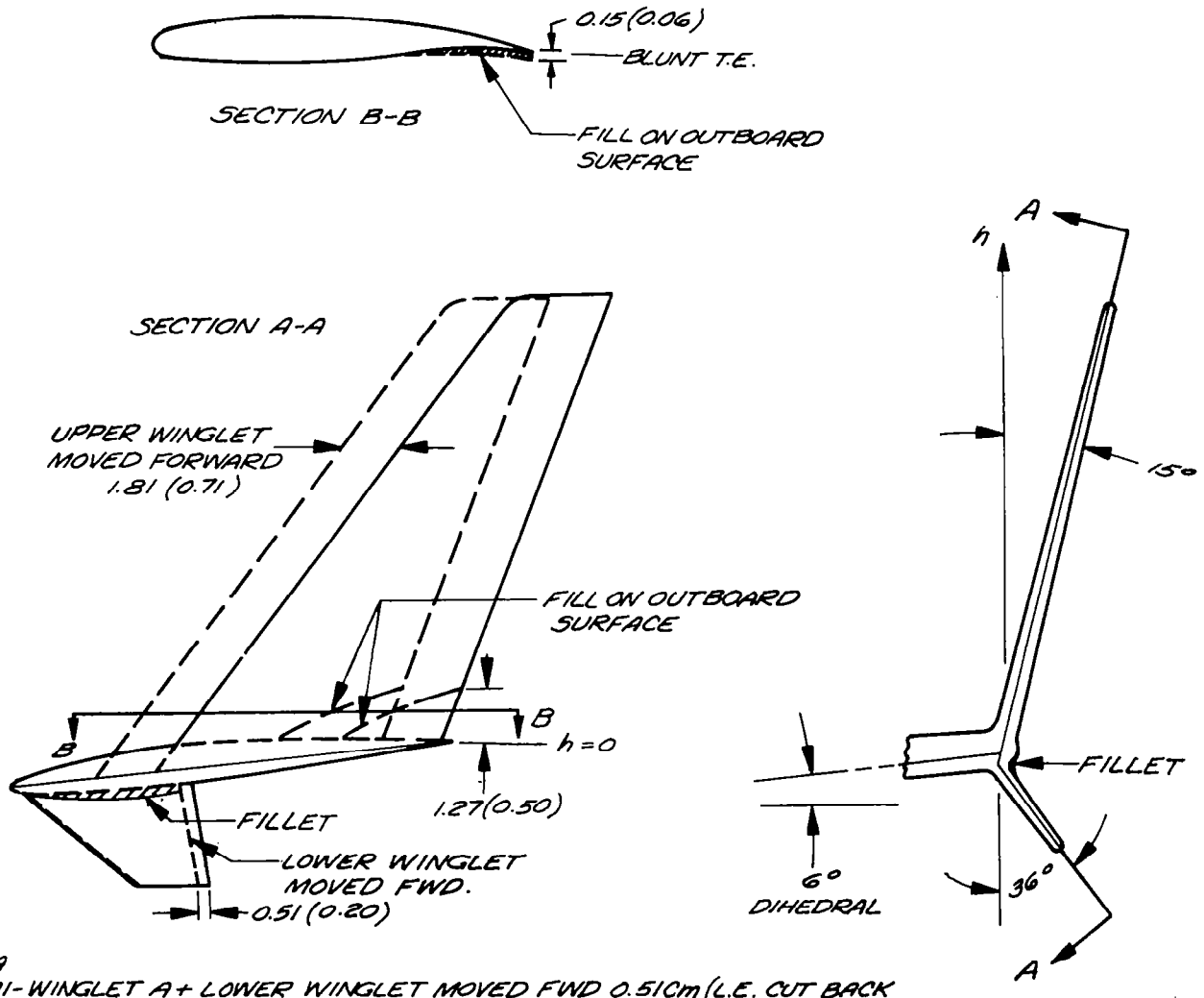

WINGLET A
WINGLET A1 - WINGLET A + LOWER WINGLET MOVED FWD 0.51Cm (L.E. CUT BACK AND RE-CONTOURED INTO WING-TIP L.E.) + LOWER WINGLET FILL
WINGLET A2 - WINGLET A1 + FILL ON UPPER WINGLET OUTBOARD SURFACE
WINGLET A3 - WINGLET A2 + UPPER SURFACE WINGLET MOVED FWD

DIMENSIONS ARE IN CENTIMETERS (INCHES)

FIGURE 9. GEOMETRY DEFINITION OF WINGLET A DEVELOPMENT CONFIGURATIONS INSTALLED ON DC-10 SERIES 10

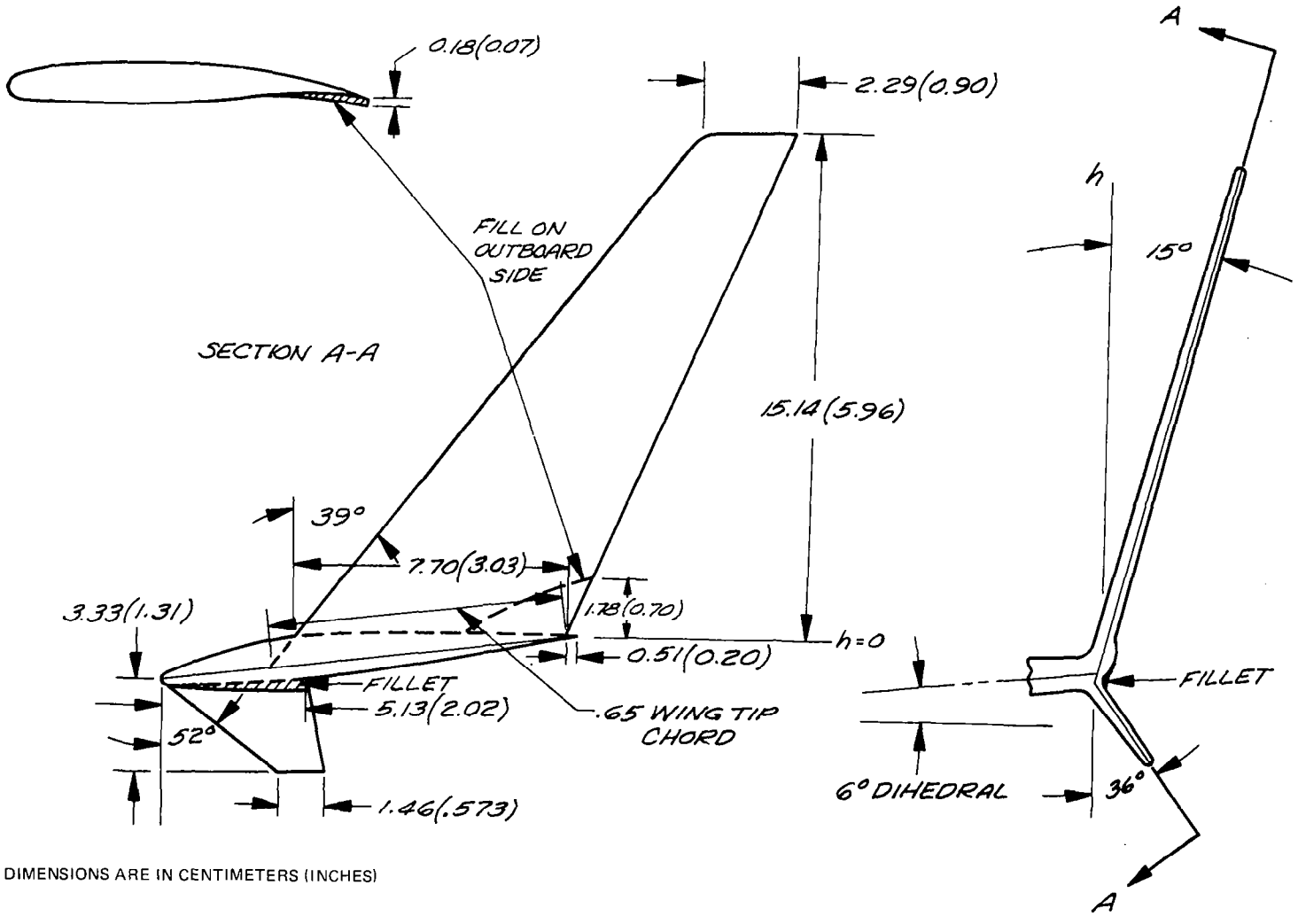

DIMENSIONS ARE IN CENTIMETERS (INCHES)

FIGURE 10. GEOMETRY DEFINITION OF WINGLET B INSTALLED ON DC-10 SERIES 30/40

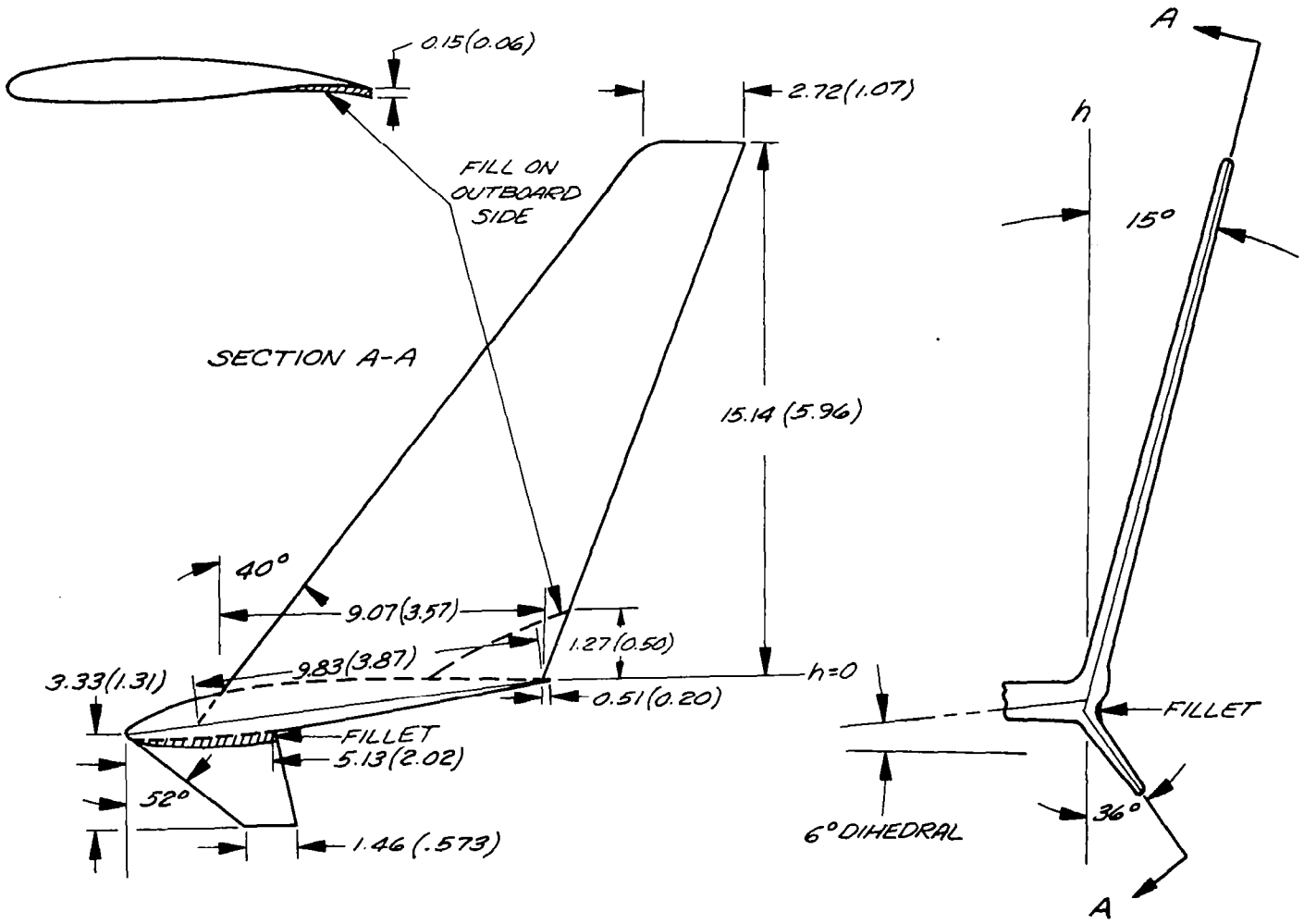

DIMENSIONS ARE IN CENTIMETERS (INCHES)

FIGURE 11. GEOMETRY DEFINITION OF WINGLET C INSTALLED ON DC-10 SERIES 30/40

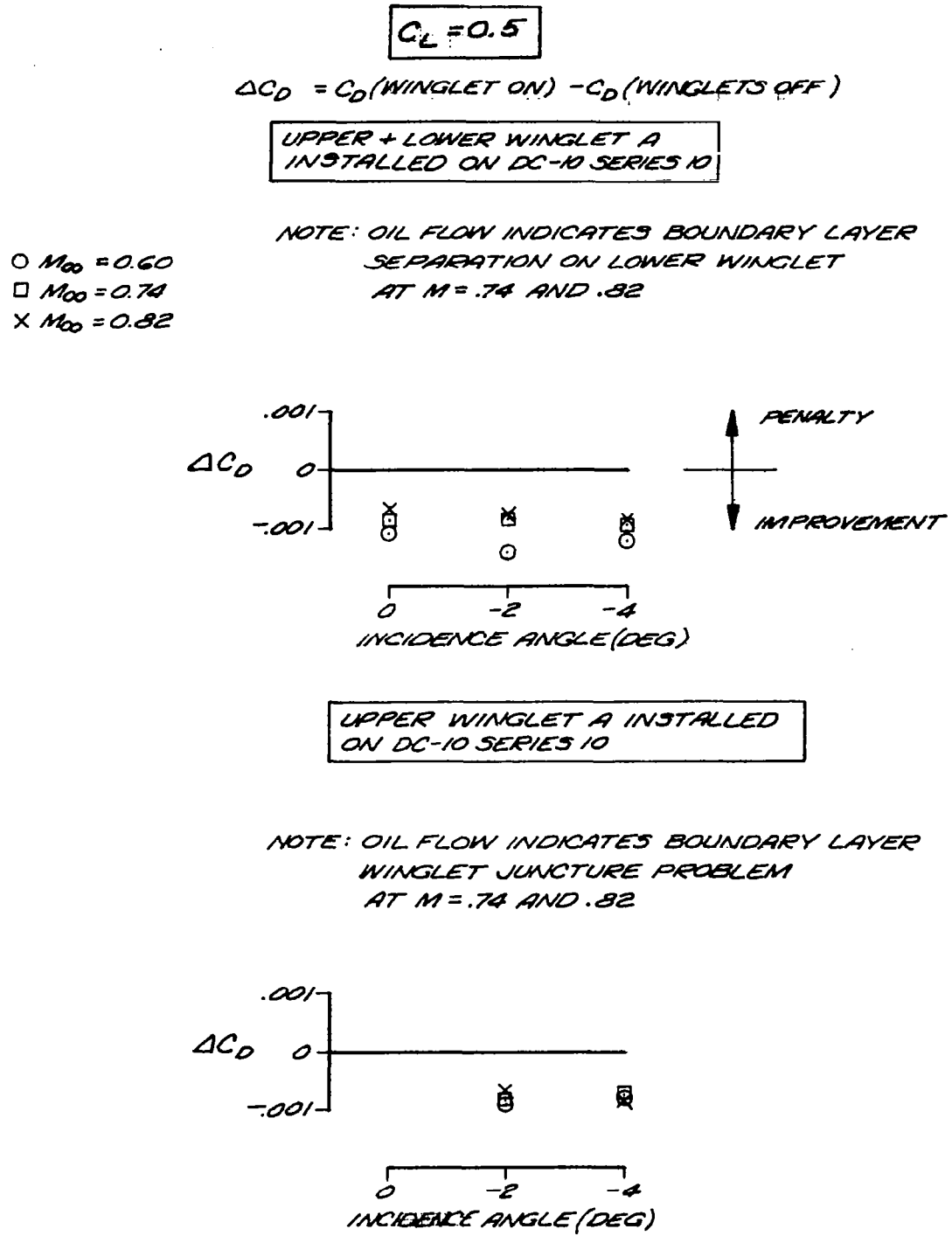

FIGURE 12. WINGLET A DEVELOPMENT ON DC-10 SERIES 10: EFFECT OF WINGLET INCIDENCE ON WINGLET INCREMENTAL DRAG IMPROVEMENT

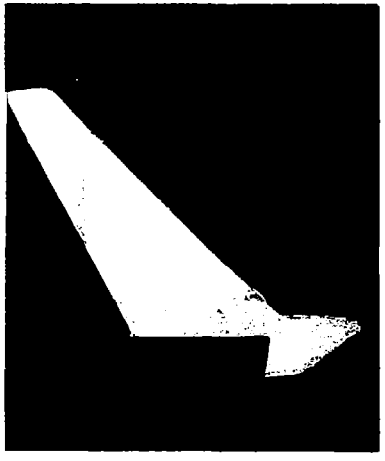

M = 0.60

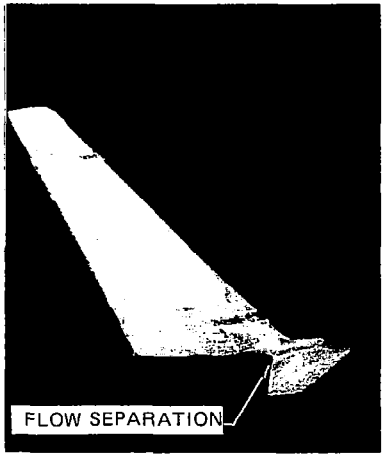

M = 0.74

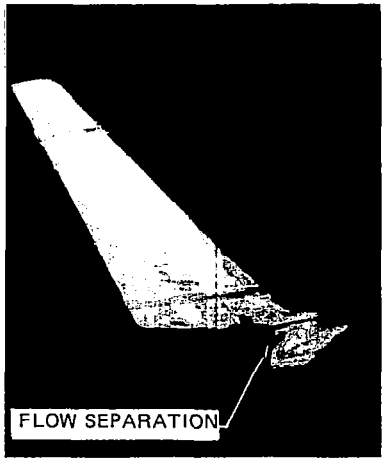

M = 0.82

UPPER AND LOWER WINGLET A

$C_L \approx 0.5$, UPPER WINGLET INCIDENCE = -2^o

M = 0.60

M = 0.74

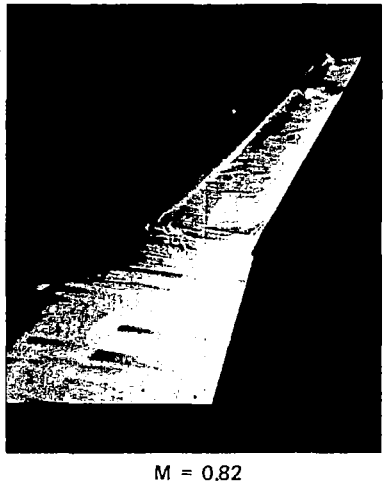

M = 0.82

$C_L \approx 0.5$, UPPER WINGLET INCIDENCE = -2^o

FIGURE 13. OIL FLOW VISUALIZATION OF WINGLET A ON DC-10 SERIES 10

WINGLET A

WINGLET A1

$M = 0.82, C_L \approx 0.5$

UPPER WINGLET INCIDENCE = -2^o

FIGURE 14. OIL FLOW VISUALIZATION OF WINGLET A DEVELOPMENT ON DC-10 SERIES 10

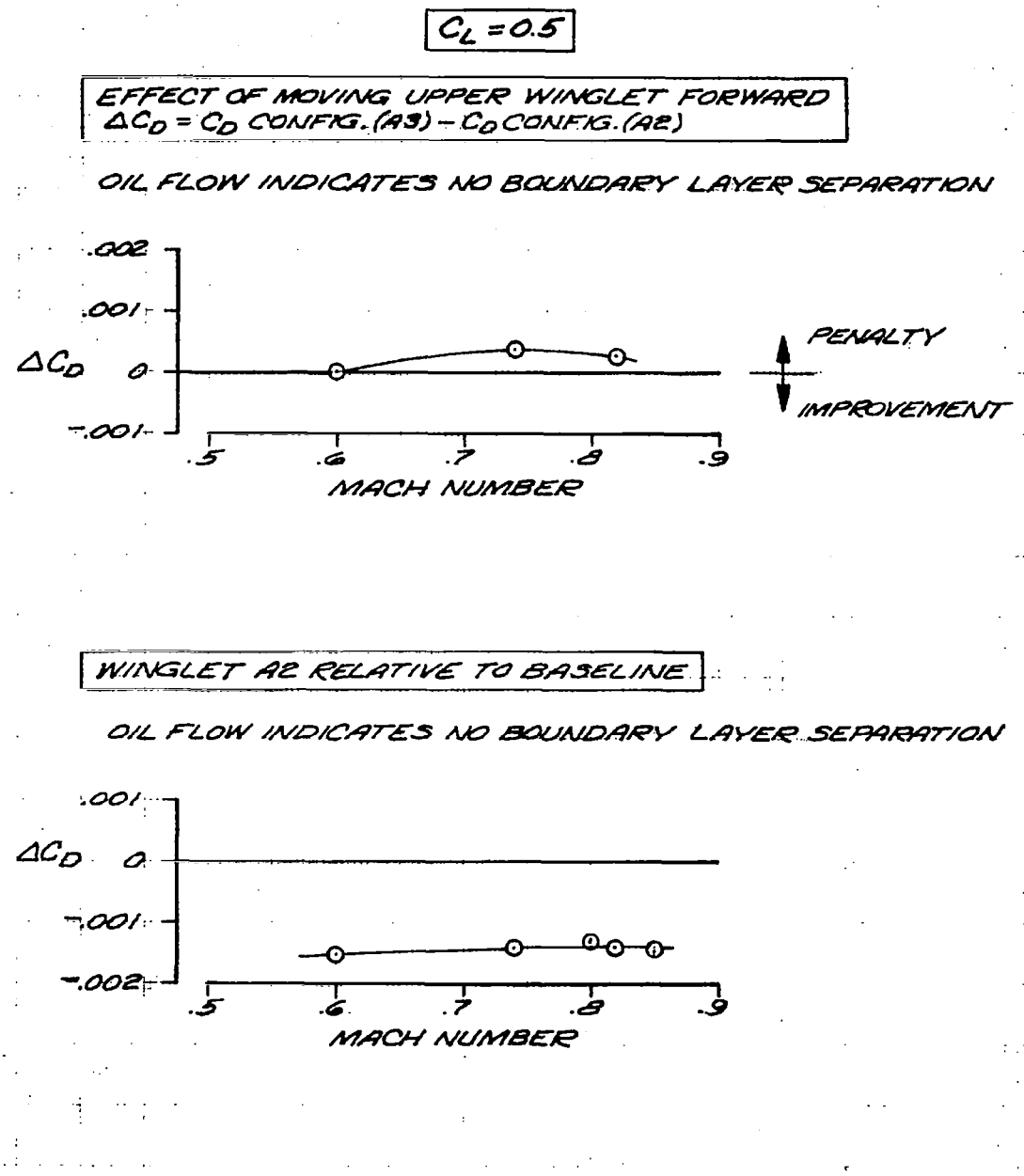

FIGURE 15. WINGLET A DEVELOPMENT ON DC-10 SERIES 10: EFFECT OF MOVING UPPER WINGLET FORWARD AND BEST WINGLET (A2) INCREMENTAL DRAG IMPROVEMENT

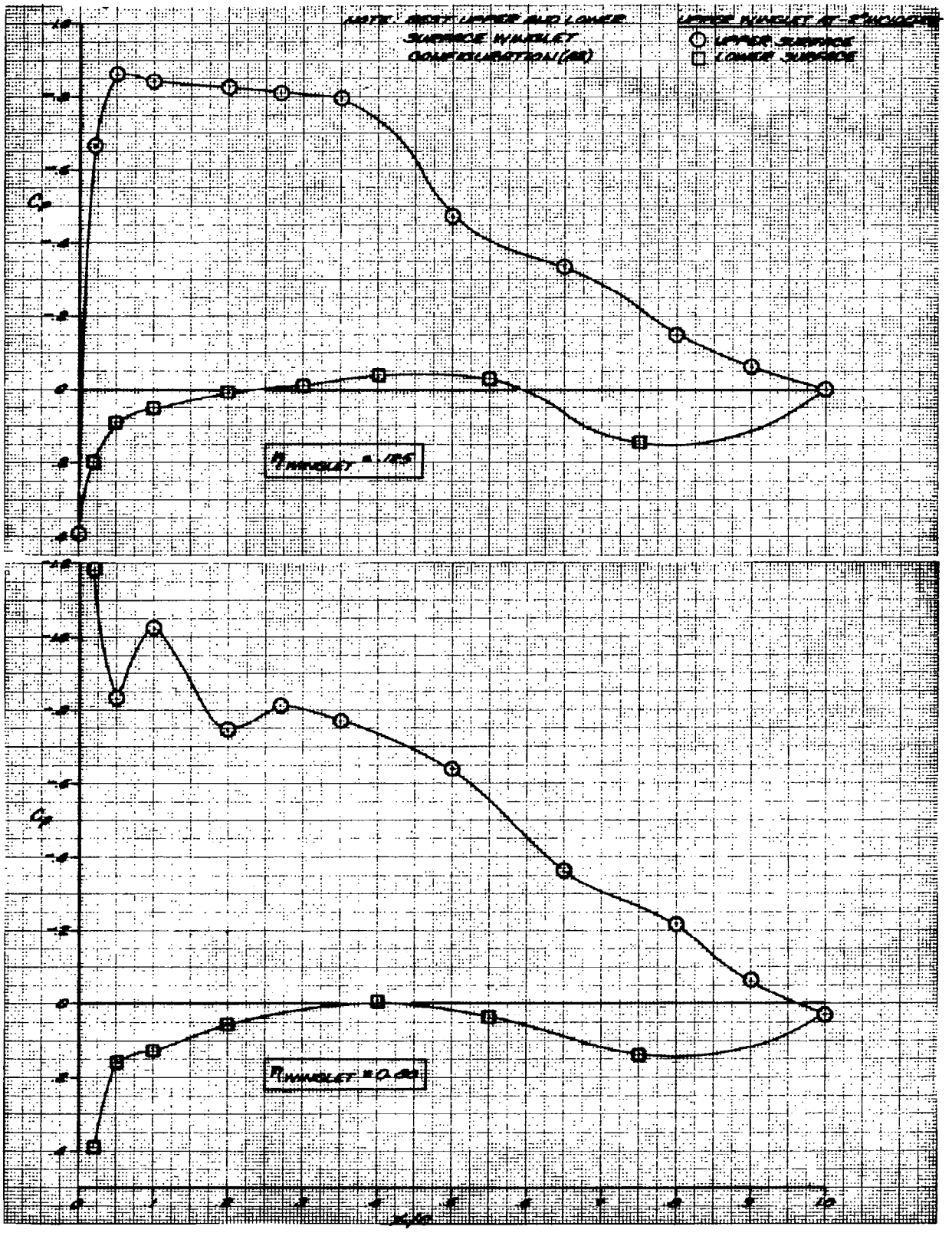

$M_\infty = 0.82,\ C_L = 0.50$

FIGURE 16. DC-10 SERIES 10 UPPER SURFACE WINGLET A2 CHORDWISE PRESSURE DISTRIBUTIONS

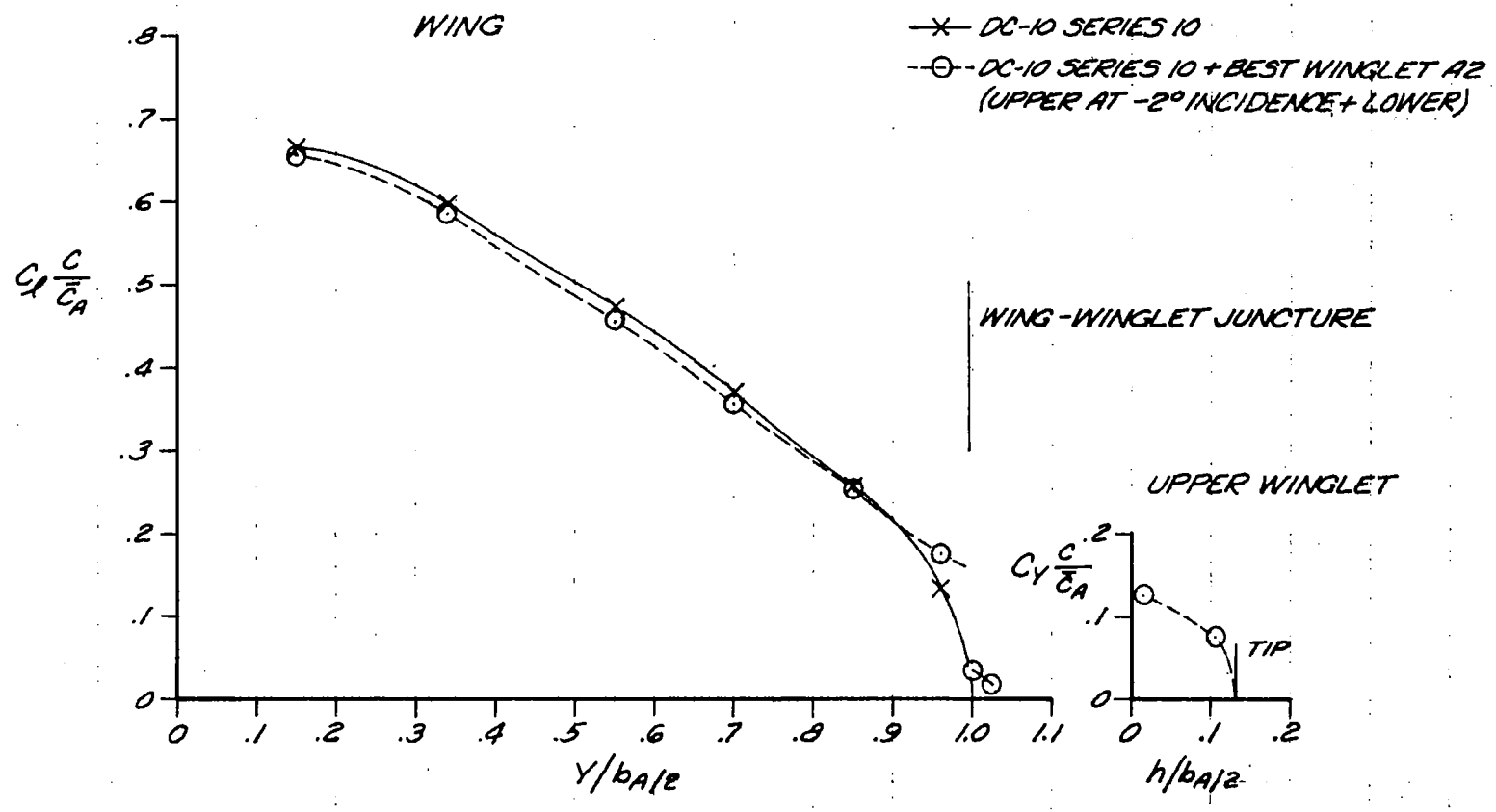

$M_\infty = 0.82$, $C_L \approx 0.5$

FIGURE 17. SPANWISE LOAD DISTRIBUTIONS FOR DC-10 SERIES 10 WITH AND WITHOUT WINGLET A2

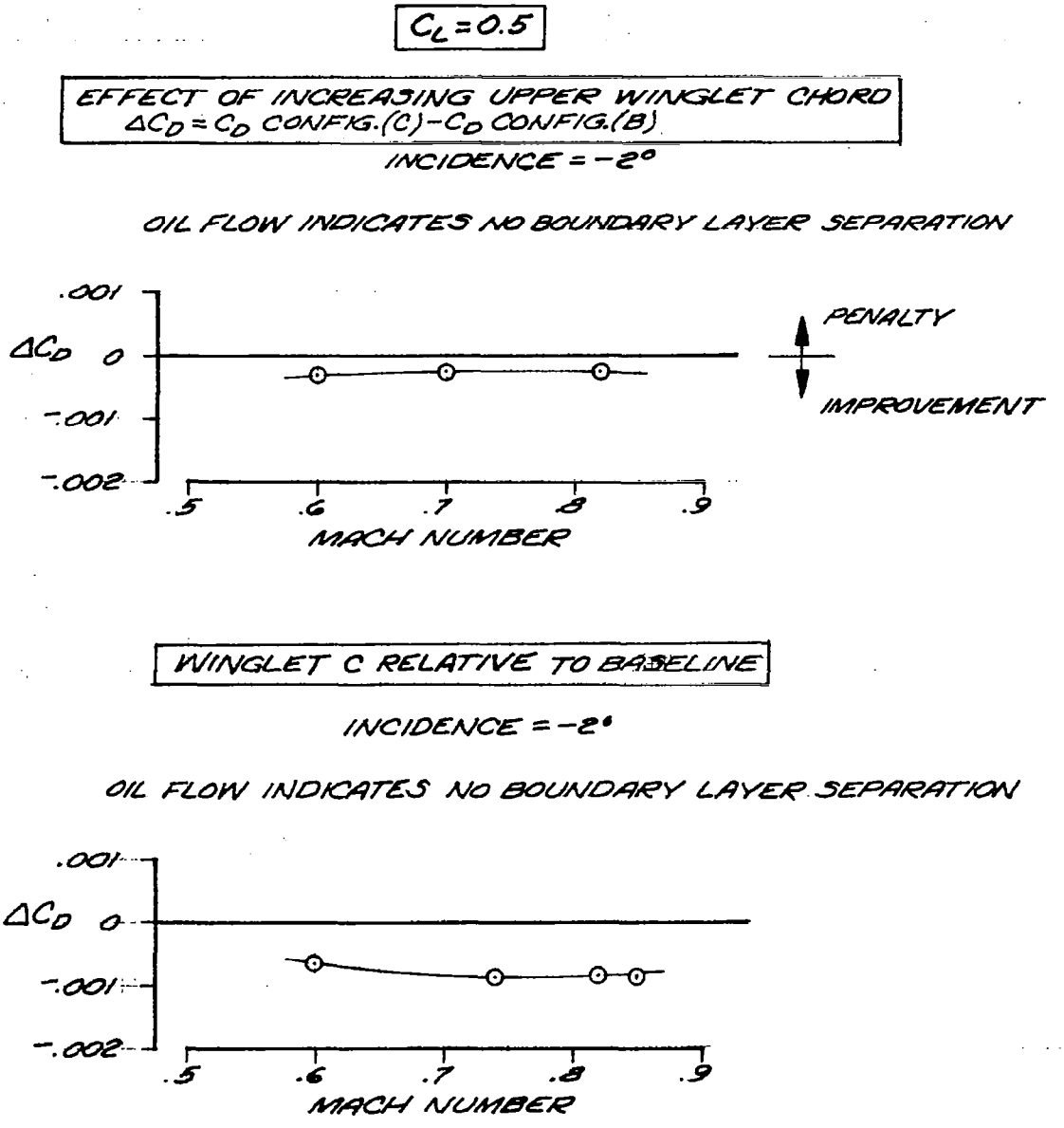

FIGURE 18. WINGLET DEVELOPMENT ON DC-10 SERIES 30/40: EFFECT OF INCREASED UPPER WINGLET CHORD AND BEST WINGLET C INCREMENTAL DRAG IMPROVEMENT

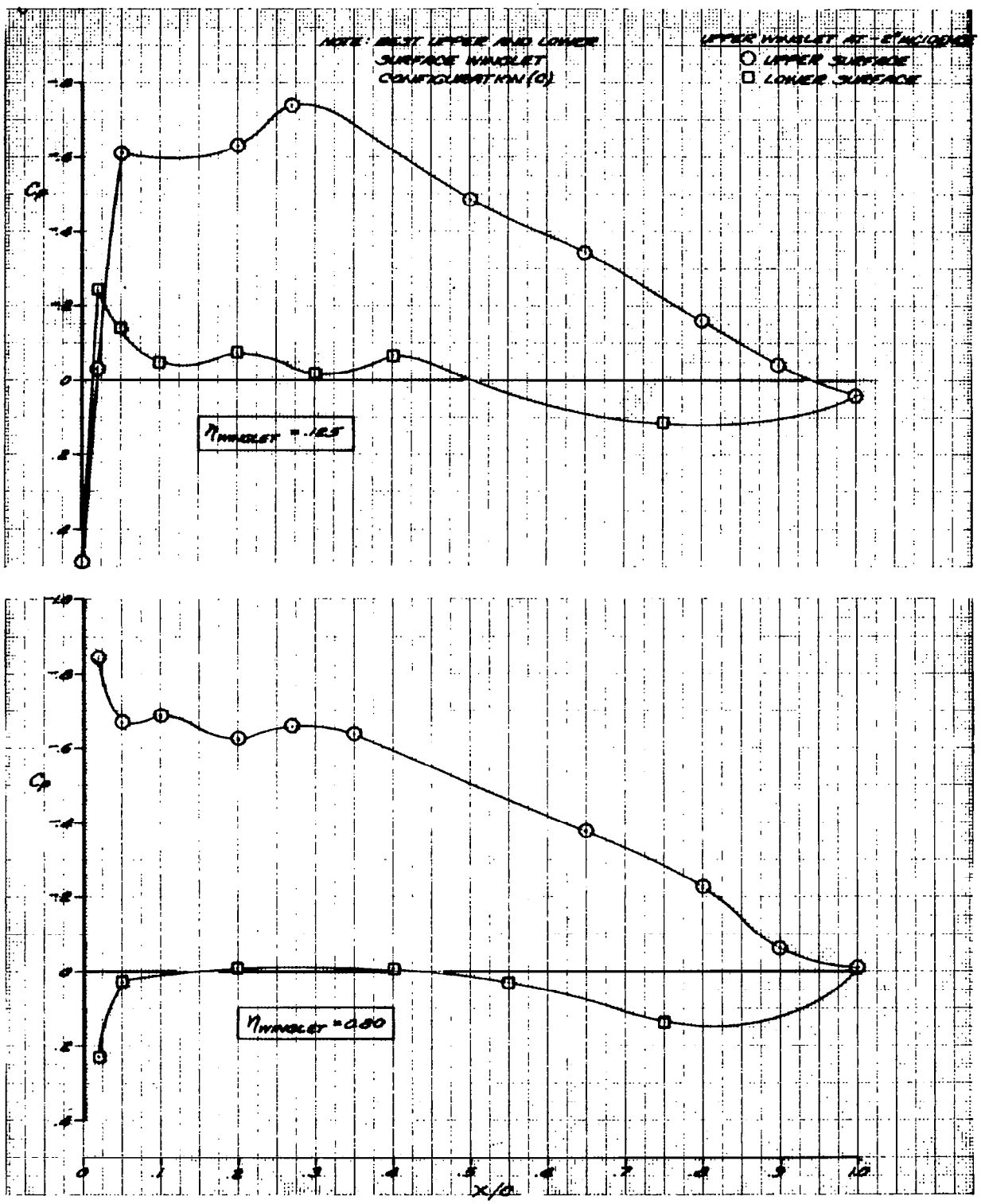

$M_\infty = 0.82$, $C_L = 0.50$

FIGURE 19. DC-10 SERIES 30/40 UPPER SURFACE WINGLET C CHORDWISE PRESSURE DISTRIBUTIONS

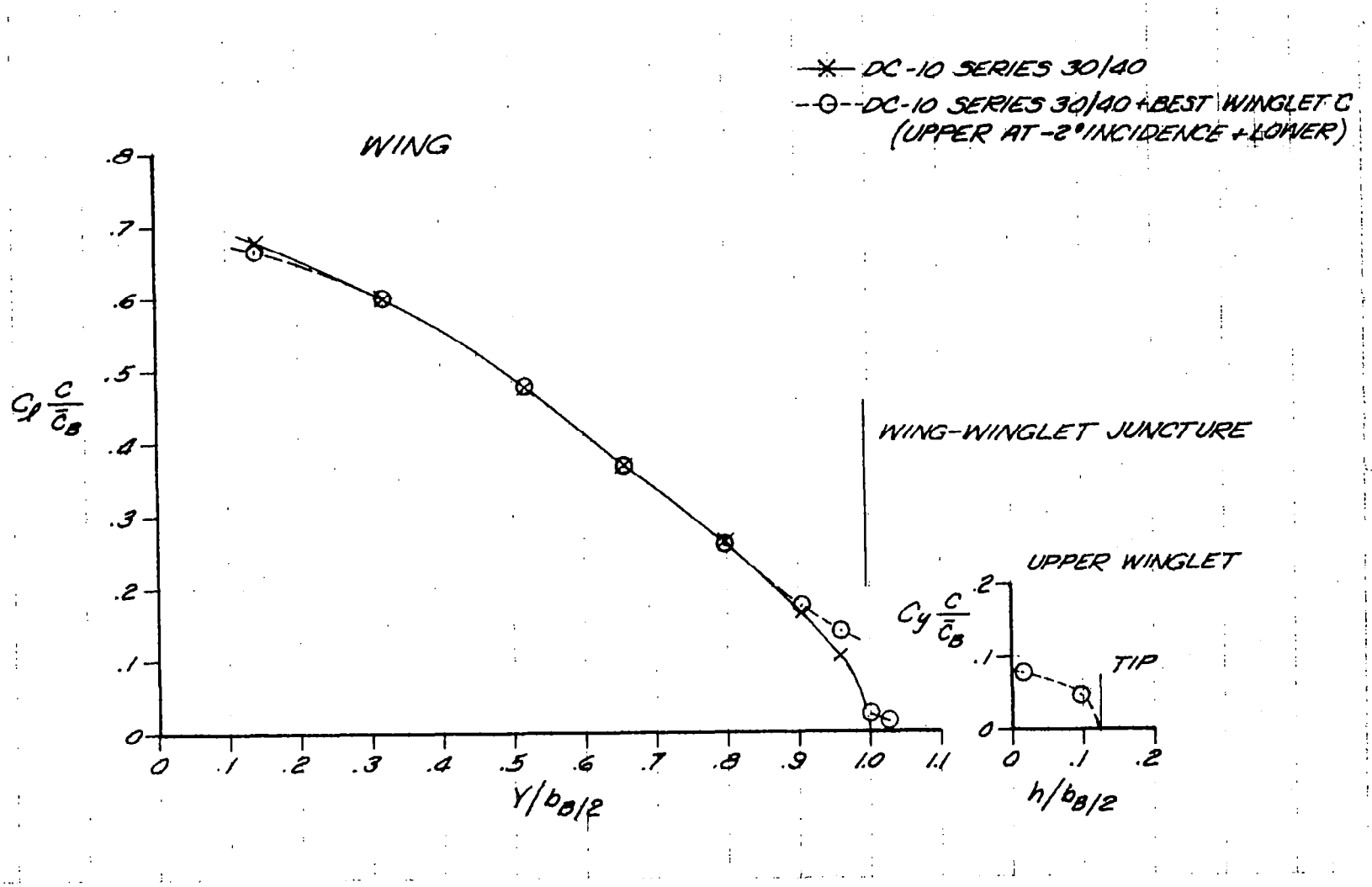

$M_\infty = 0.82$, $C_L \approx 0.5$

FIGURE 20. SPANWISE LOAD DISTRIBUTIONS FOR DC-10 SERIES 30/40 WITH AND WITHOUT WINGLET C

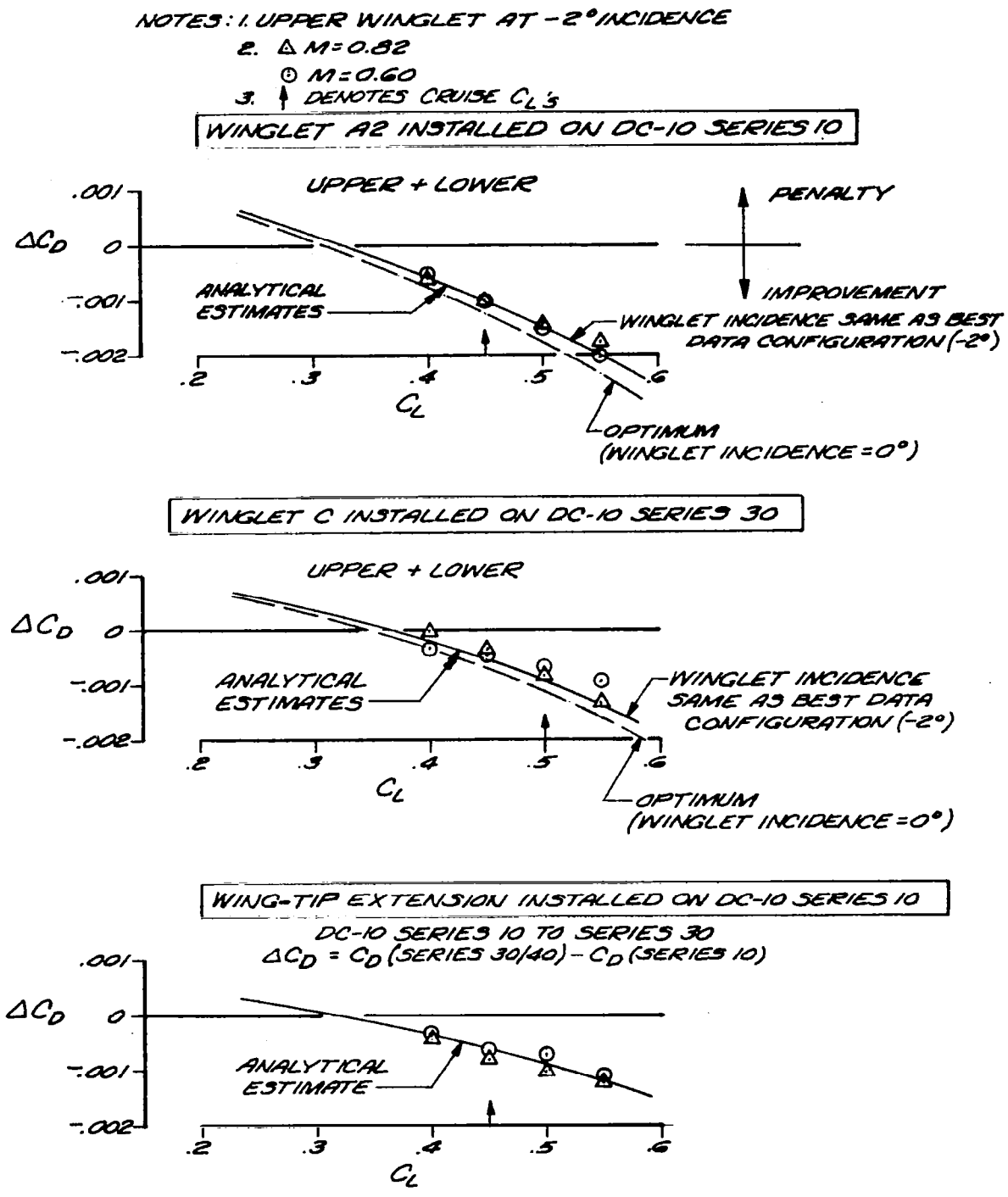

FIGURE 21. SUMMARY COMPARISON: EFFECT OF BEST WINGLET INSTALLATIONS AND WING-TIP INSTALLATION ON INCREMENTAL CRUISE DRAG

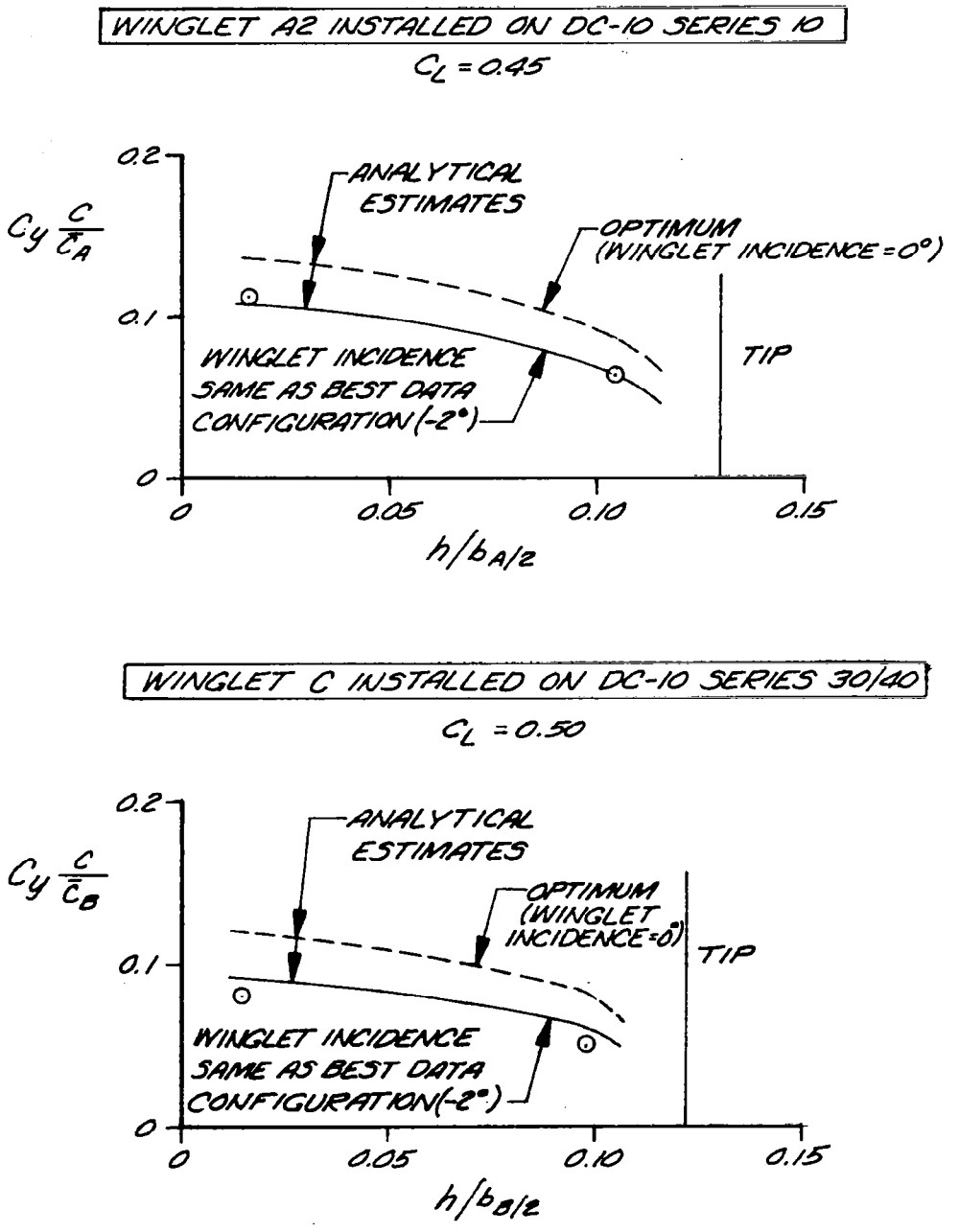

M = 0.82

FIGURE 22. WINGLET LOADINGS COMPARED WITH ANALYTICAL ESTIMATES

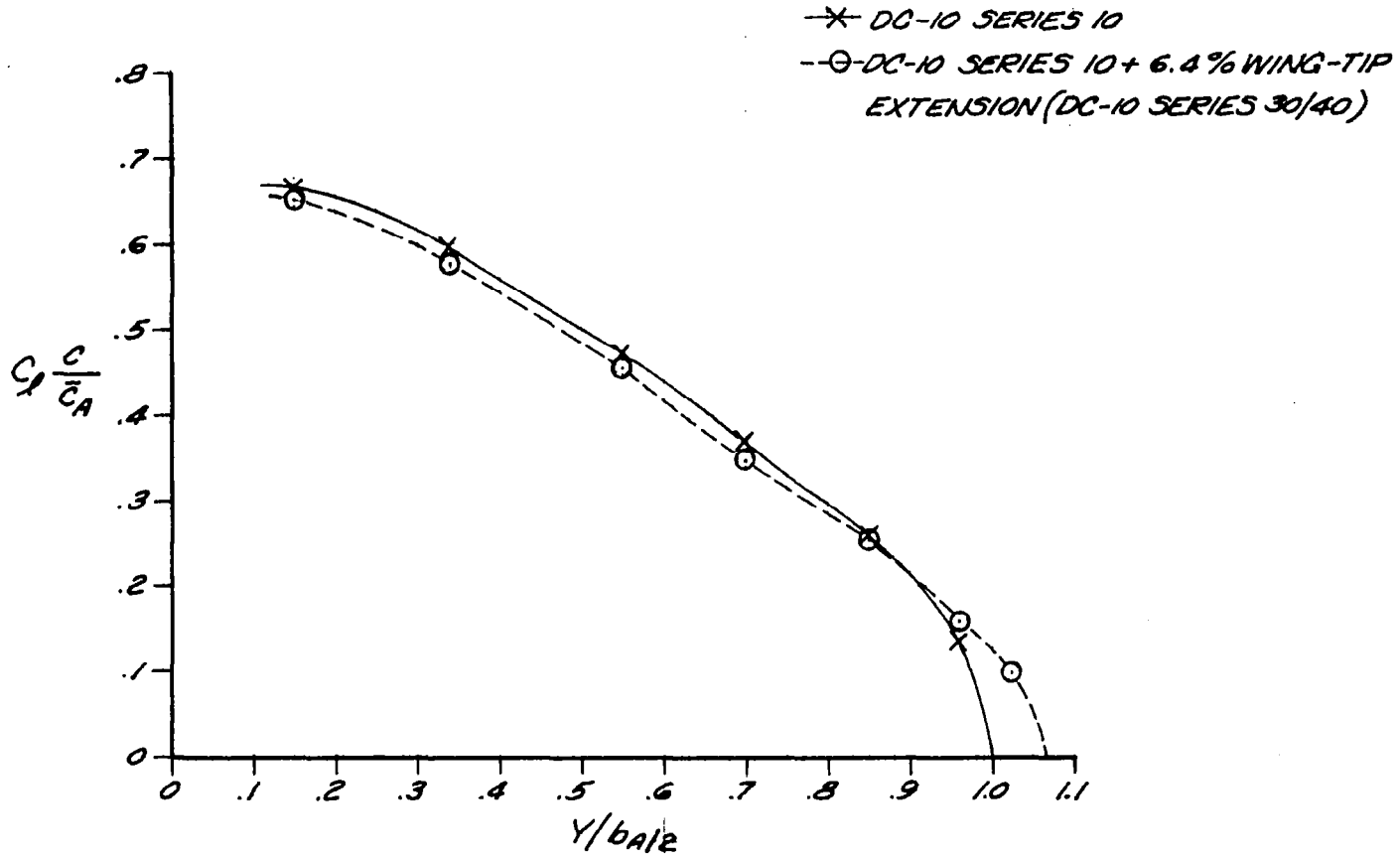

$M_\infty = 0.82$, $C_L \approx 0.5$

FIGURE 23. WING SPANWISE LOAD DISTRIBUTIONS FOR DC-10 SERIES 10 AND 30/40

WIND TUNNEL REYNOLDS NUMBER

	DC-10 SERIES 10 WINGLET A2 CRUISE $C_L = 0.45$	DC-10 SERIES 10 + 6.4% WING-TIP EXT. CRUISE $C_L = 0.45$	DC-10-30/40 WINGLET C CRUISE $C_L = 0.50$
M	ΔC_D	ΔC_D	ΔC_D
.60	−.00099	−.00062	−.00067
.68	N/A	−.00058	N/A
.74	−.00092	−.00064	−.00091
.80	−.00096	−.00056	N/A
.82	−.00100	−.00081	−.00085
.85	−.00092	−.00077	−.00086

ADJUSTED TO FLIGHT REYNOLDS NUMBER

M	ΔC_D	ΔC_D	ΔC_D
.60	−.00119	−.00071	−.00086
.68	N/A	−.00067	N/A
.74	−.00112	−.00073	−.00110
.80	−.00116	−.00065	N/A
.82	−.00120	−.00090	−.00104
.85	−.00112	−.00086	−.00105

FIGURE 24. WINGLETS AND WING-TIP EXTENSION INCREMENTAL CRUISE DRAG DATA SUMMARY

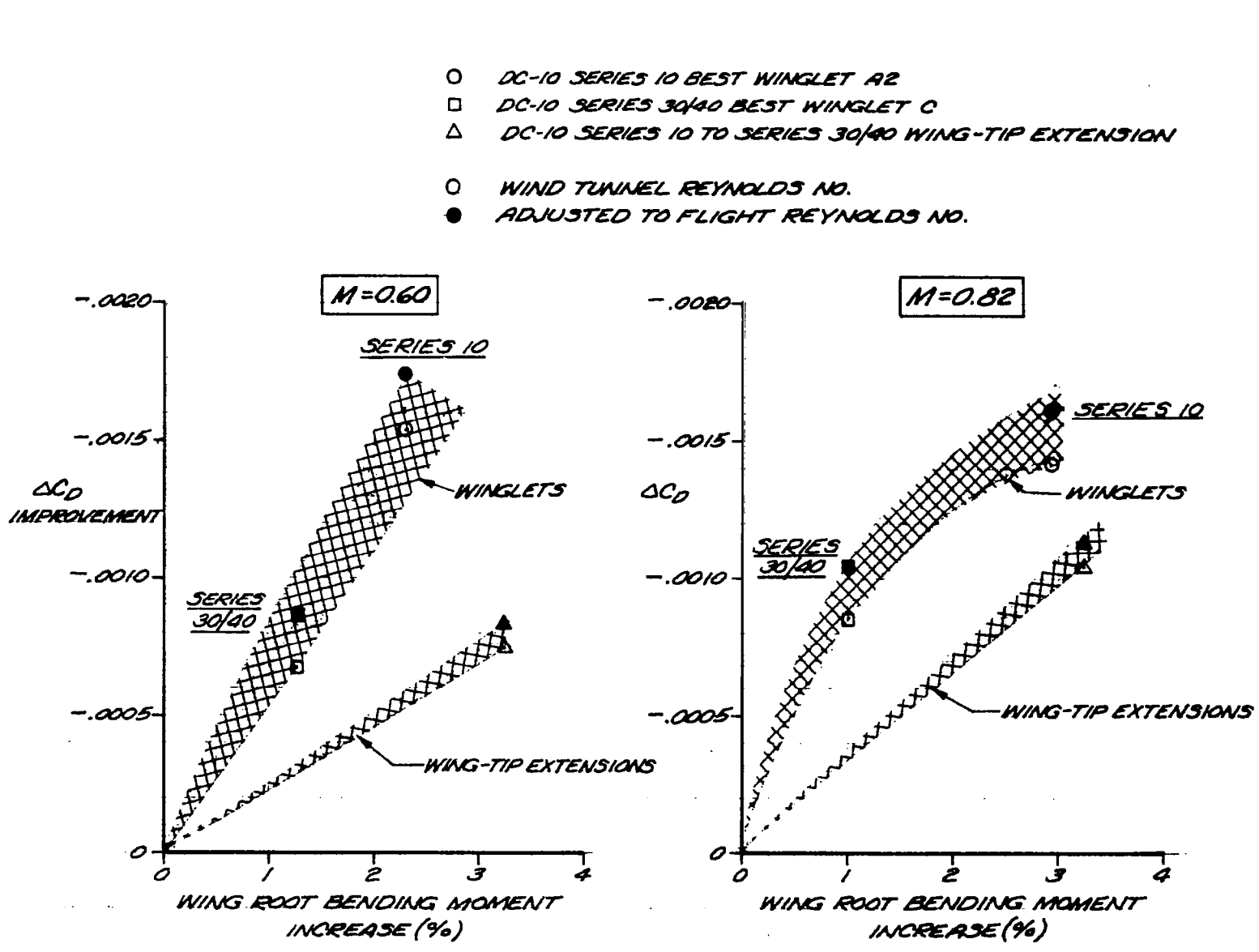

$C_L = 0.50$

FIGURE 25. COMPARISON OF WINGLETS AND WING-TIP EXTENSION EFFECTS ON INCREMENTAL CRUISE DRAG AND WING ROOT BENDING MOMENT

1. Report No.	2. Government Accession No.	3. Recipient's Catalog No.
NASA CR-3119		

4. Title and Subtitle	5. Report Date
Design and Wind Tunnel Tests of Winglets on a DC-10 Wing	April 1979
	6. Performing Organization Code: ACEE-05-FR-8423

7. Author(s)	8. Performing Organization Report No.
R. D. Gilkey	
	10. Work Unit No.

9. Performing Organization Name and Address	11. Contract or Grant No.
Douglas Aircraft Company McDonnell Douglas Corporation 3855 Lakewood Boulevard Long Beach, California 90846	NAS1-14743
	13. Type of Report and Period Covered: Contractor Report

12. Sponsoring Agency Name and Address	14. Sponsoring Agency Code
National Aeronautics and Space Administration Washington, D.C. 20546	

15. Supplementary Notes

Technical Representative of the Contracting Officer, Donald L. Maiden, Energy Efficient Transport Project, NASA Langley Research Center, Hampton, Virginia 23665

Final Report

16. Abstract

This report presents the results of a wind tunnel test utilizing a 4.7 percent scale semi-span model in the Langley Research Center 8-foot transonic pressure wind tunnel to establish the cruise drag improvement potential of winglets as applied to the DC-10 wide body transport aircraft. Winglets were investigated on both the DC-10 Series 10 (domestic) and 30/40 (intercontinental) configurations and compared with the Series 30/40 configuration. The results of the investigation confirm that for the DC-10, winglets provide approximately twice the cruise drag reduction of wing-tip extensions for about the same increase in bending moment at the wing-fuselage juncture. Furthermore, the winglet configurations achieved drag improvements which were in close agreement to analytical estimates. It was observed that relatively small changes in wing-winglet tailoring effected large improvements in drag and visual flow characteristics. All final winglet configurations exhibited good visual flow characteristics on the wing and winglets.

17. Key Words (Suggested by Author(s))	18. Distribution Statement
Winglets Wing-tip extensions Cruise drag reduction Wing bending moment	FEDD Distribution

19. Security Classif. (of this report)	20. Security Classif. (of this page)	21. No. of Pages	22. Price*
Unclassified	Unclassified	49	